Therapeutic suppression of proteolipid protein rescues Pelizaeus-Merzbacher Disease in mice

Matthew S. Elitt[1], Lilianne Barbar[1], H. Elizabeth Shick[1], Berit E. Powers[2], Yuka Maeno-Hikichi[1], Mayur Madhavan[1], Kevin C. Allan[1], Baraa S. Nawash[1], Zachary S. Nevin[1], Hannah E. Olsen[1], Midori Hitomi[3], David F. LePage[1], Weihong Jiang[1], Ronald A. Conlon[1], Frank Rigo[2], Paul J. Tesar[1*]

[1]Department of Genetics and Genome Sciences, Case Western Reserve University School of Medicine, Cleveland, Ohio 44106, USA.
[2]Ionis Pharmaceuticals, Carlsbad, California 92008, USA.
[3]Lerner Research Institute, Cleveland Clinic Foundation, Cleveland, Ohio 44106, USA.

*email: paul.tesar@case.edu

Mutations in *proteolipid protein 1* (*PLP1*) result in failure of myelination and severe neurological dysfunction in the X-linked pediatric leukodystrophy Pelizaeus-Merzbacher disease (PMD). The majority of *PLP1* variants, including supernumerary copies and various point mutations, lead to early mortality. However, *PLP1*-null patients and mice display comparatively mild phenotypes, suggesting that reduction of aberrant *PLP1* expression might provide a therapeutic strategy across PMD genotypes. Here we show, CRISPR-Cas9 mediated germline knockdown of *Plp1* in the severe *jimpy* (*Plp1*[jp]) point mutation mouse model of PMD rescued myelinating oligodendrocytes, nerve conduction velocity, motor function, and lifespan to wild-type levels, thereby validating *PLP1* suppression as a therapeutic approach. To evaluate the therapeutic potential of *Plp1* suppression in postnatal PMD mice, we tested antisense oligonucleotides (ASOs) that stably decrease mouse *Plp1* mRNA and protein *in vivo*. Administration of a single intraventricular dose of *Plp1*-targeted ASOs to postnatal *jimpy* mice increased myelination, improved motor behavior, and extended lifespan through an 8-month endpoint. Collectively, these results support the development of *PLP1* suppression as a disease-modifying therapy for most PMD patients. More broadly, we demonstrate that RNA therapeutics can be delivered to oligodendrocytes *in vivo* to modulate neurological function and lifespan, opening a new treatment modality for myelin disorders.

Main text:

Pelizaeus-Merzbacher disease (PMD; OMIM 312080) is an X-linked leukodystrophy typified by extensive hypomyelination of the central nervous system (CNS). Symptoms typically present early in childhood with a constellation of nystagmus, spasticity, hypotonia, and cognitive dysfunction, leading to mortality in early adulthood. In severe forms, symptoms present connatally and patients succumb to their disease in early childhood. Despite intense interest in PMD therapeutic development, including several clinical trials, no disease modifying therapies have proven efficacious in patients [1-6].

Mutations in the *proteolipid protein 1* (*PLP1;* OMIM 300401) gene underlie the pathogenesis of PMD, with variability in disease onset and progression dictated by the severity of the particular mutation [7-9]. *PLP1* codes for the tetraspan protein PLP as well as its shorter splice isoform DM20, which lacks 35 amino acids in the cytosolic loop region [10]. PLP/DM20 is highly conserved across species, with human, mouse, and rat sharing identical amino acid sequence [11]. Expression of *PLP1* is largely restricted to myelinating oligodendrocytes, where it is responsible for ~50% of the total protein content of myelin [12].

The majority of PMD cases result from duplications in *PLP1* yielding overexpression of otherwise normal PLP protein [8]. Additionally, hundreds of unique point mutations in *PLP1* which each generate abnormal PLP protein have also been discovered in patients with severe disease. Interestingly, while *PLP1* deletions are uncommon, null patients and mice display symptoms that are significantly delayed and more mild compared to those with duplications or point mutations [13-15]. Null patients can live until 40-60 years old [8,16], do not develop lower body spastic paraparesis until the second or third decade of life, and do not demonstrate cognitive regression until the third or fourth decade of life (see Extended Data Table 1 for detailed clinical presentations of *PLP1*-null patients from published reports).

58   Collectively, this clinical landscape provides several potential opportunities for therapeutic

59   development. While never tested, knockout or suppression of the duplicated copy of *PLP1* should,

60   in theory, correct elevated protein expression to normal levels in patients harboring duplications.

61   More globally, we suggest that the mild presentation of null patients provides rationale for a

62   generalized *PLP1* suppression strategy that may provide clinical benefit beyond this single use

63   case. Such an approach would provide comprehensive therapy to include the litany of point

64   mutations that generate abnormal PLP protein, abrogating the need for personalized therapy

65   tailored to each patient's severe, individual mutation.

66   To test this latter strategy, we evaluated *Plp1* suppression as a therapeutic approach for

67   PMD using the *jimpy* (*Plp1^jp^*) mouse, which expresses a mutant PLP protein due to a point

68   mutation in splice acceptor site of intron 4 of *Plp1*, leading to exon 5 skipping and a frameshift

69   affecting the final 70 amino acids in the C-terminus of PLP/DM20. *Jimpy* mice exhibit severe

70   neurological symptoms, die at 3 weeks of age, and accurately reflect the cellular and molecular

71   pathology seen in human disease. To test if *Plp1* suppression was a valid therapeutic strategy for

72   PMD we first utilized nuclease-mediated cleavage of DNA by clustered regularly interspaced short

73   palindromic repeat-associated 9 (CRISPR-Cas9) protein [17,18] with synthetic guide RNAs (sgRNA)

74   targeted to induce a frameshift in PLP1 exon 3 and trigger subsequent knockdown of *Plp1* mRNA

75   by nonsense-mediated decay. *Plp1*-targeting sgRNAs were designed and tested for on-target

76   cutting efficiency and two sgRNAs (3 and 7) were administered to knockdown *Plp1* by germline

77   editing of *jimpy* mice (Fig. 1a). Concomitant administration of both sgRNAs with Cas9 mRNA

78   from Streptococcus pyogenes (spCas9) in zygotes from crosses of *jimpy*-carrier females with wild-

79   type males generated mice with high on-target mutation efficiency in *Plp1* (Extended Data Fig.

80   1a). These founders included a *jimpy* male with complex deletion of 80 total nucleotides of DNA

3

81   in exon 3 of his single copy of *Plp1* on the X chromosome, resulting in a frameshift in exon 3 and

82   an early termination codon in exon 4 (Fig. 1a and Extended Data Fig. 1b). This mouse denoted

83   "CR-*impy*" (for CRISPR frameshift-mediated knockdown of *Plp1* in *jimpy*) showed no overt

84   neurological phenotypes. A line of CR-*impy* was bred to evaluate cellular, molecular, and

85   functional phenotypes, along with contemporaneous, isogenic wild-type and *jimpy* male mice.

86   As expected *jimpy* males displayed the typical pathological phenotypes including severe

87   tremor, ataxia, seizures (lasting >30 seconds), and death by the third postnatal week (Fig. 1b,

88   Supplementary Fig. 1, Supplementary Video 1). In contrast, CR-*impy* mice, which had a 61-74%

89   reduction *Plp1* transcript expression in multiple brain regions (Extended Data Fig. 1c), showed a

90   21-fold increase in lifespan (mean survival = 23 and 489 days in *jimpy* and CR-*impy*, respectively)

91   with no overt tremor, ataxia, or evidence of seizures through the terminal endpoint at 18 months

92   of age (Fig. 1b, Supplementary Fig. 1, Supplementary Video 1, and Supplementary Video 2).

93   Assessment of CR-*impy* mice at 3 weeks, 6 months, and 18 months of age by

94   immunohistochemistry revealed a stable restoration of oligodendrocytes to near wild-type levels

95   throughout the neuraxis, as evidenced by expression of the mature myelin marker myelin basic

96   protein (MBP), and quantification of oligodendrocyte number using the oligodendrocyte-specific

97   transcription factor myelin regulatory factor (MyRF) (Fig. 1c-e). Quantification of MBP protein

98   by western blot and RNA by qRT-PCR further supported these findings, revealing 40-95%

99   restoration of MBP at 3 weeks and full restoration of *Mbp* expression and MBP at 6 months of age

100   across multiple brain regions in CR-*impy* mice compared to wild-type (Extended Data Fig. 1d-f).

101   Restoration of oligodendrocytes in CR-*impy* mice grossly reduced reactivity of microglia and

102   astrocytes normally seen in *jimpy* mice at 3 weeks of age, and was sustained into adulthood

103   (Extended Data Fig. 2a, b). Finally, MBP+ CR-*impy* oligodendrocytes ensheathed phospho-

104   neurofilament+ axons in a similar manner to wild-type samples (Fig. 1f), suggestive of a

105   potentially comparable myelination status.

106   Electron micrographs and tissue sections stained with toluidine blue demonstrated

107   increased myelination in CR-*impy* mice. Examination of optic nerves, which provide

108   straightforward quantification of myelination from aligned axons, revealed a significant 6-fold

109   improvement in the number and density of myelinated axons in CR-*impy* animals, reaching 53%

110   of wild-type levels at 3 weeks of age (Fig. 1g, h, and Extended Data Fig. 3a). Myelination in CR-

111   *impy* animals was sustained through 6 month and 18 month time points, approaching wild-type

112   levels (Fig. 1i and Extended Data Fig. 3b, c). Additionally, examination of corpus callosum myelin

113   at 3 weeks (Extended Data Fig. 3d) further revealed that these improvements were not restricted

114   to the optic nerve but manifested throughout the neuraxis of CR-*impy* mice.

115   Although the quantity of myelin increased drastically compared to *jimpy*, we noted that

116   CR-*impy* myelin sheaths were not quite as compact as those seen in age-matched wild type

117   controls. To determine if restored myelin in CR-*impy* mice was functional we used

118   electrophysiology to measure conduction velocity in the optic nerve at two time points. At 3 weeks

119   of age we found a significant 2.6- and 1.7-fold increase in 1st and 2nd peak conduction velocities,

120   respectively, in CR-*impy* mice compared to *jimpy*. Intriguingly, these values trailed wild-type

121   conduction velocities, a finding consistent with our quantitative electron microscopy showing an

122   incomplete restoration of myelinated axons at the 3 week time point. However, over time this

123   discrepancy disappeared and by 6 months of age we found no significant difference in optic nerve

124   conduction velocity in CR-*impy* mice relative to wild-type (Fig. 2a, b), suggesting that suppression

125   of *Plp1* does not impair myelin function.

126   Finally, we wanted to determine if the widespread restoration of CR-*impy* oligodendrocytes

127 resulted in a meaningful recovery of motor performance using the accelerating rotarod and open

128 field behavioral assays at 3 weeks, 2 months, 6 months, and 18 months of age. In rotarod testing,

129 which measures motor learning, function, and coordination, CR-*impy* mice showed equivalent

130 performance to wild-type up through 6 months of age. At the final 18 month time point we noted

131 a slight decrease in CR-*impy* performance relative to wild-type (Fig. 2c). This is consistent with

132 prior reports in mice with complete *Plp1* knockout in otherwise wild-type mice, which showed a

133 decline in rotarod performance in late adulthood relative to wild-type due to long tract axon

134 degeneration [13]. Overall locomotion of CR-*impy* mice in open field testing was equivalent to wild-

135 type at all time points tested (Fig. 2d). Together, these results establish that frameshift-mediated

136 knockdown of mutant *Plp1* in PMD mice prevents disease with near complete restoration of

137 oligodendrocytes, functional myelin, and lifespan.

138   PMD is thought to result from a cell-intrinsic deficit within the oligodendrocyte lineage [19-

139 23]. In the CNS, PLP (protein) is restricted to oligodendrocytes, but *Plp1* transcript and transgene

140 expression have been reported in a few neuronal subsets [24]. Since CR-*impy* mice have constitutive

141 germline *Plp1* knockdown in all cells, we generated and validated induced pluripotent stem cells

142 (iPSCs) from isogenic wild-type, CR-*impy*, and *jimpy* mice (Extended Data Fig. 4a, b) to generate

143 pure populations of oligodendrocyte progenitor cells (OPCs) and assess the cell type specific effect

144 of *Plp1* knockdown, *in vitro* [25,26]. OPCs expressing the canonical transcription factors Olig2 and

145 Sox10 (Extended Data Fig. 4c, d) were stimulated to differentiate towards an oligodendrocyte fate

146 by addition of thyroid hormone, and MBP+ oligodendrocytes were quantified. As expected [22],

147 *jimpy* cultures contained only rare surviving MBP+ oligodendrocytes with a concomitant loss in

148 total cells (Fig. 3a-c). In contrast CR-*impy* cultures showed a complete rescue of MBP+

149   oligodendrocytes as well as total cells (Fig. 3a-c). These results suggest that oligodendrocyte

150   restoration in CR-*impy* mice is due to an amelioration of intrinsic cellular pathology within the

151   oligodendrocyte lineage.

152   After genetically validating *Plp1* knockdown as a therapeutic target for disease-

153   modification in PMD, we pursued a clinically translatable strategy for *in vivo*, postnatal

154   suppression of *Plp1*. While postnatal delivery of CRISPR-based therapeutics has demonstrated

155   pre-clinical efficacy in a separate CNS disorder [27], delivery challenges, off-target risks [28,29], and

156   the potential to generate more severe, in-frame mutations due to imprecise repair [30,31] led us to

157   employ anti-sense oligonucleotides (ASOs) to test suppression of *Plp1*. ASOs are short single-

158   stranded oligodeoxynucleotides with chemical modifications that confer enhanced

159   pharmacological properties including robust *in vivo* stability, target affinity, and cellular uptake

160   when delivered directly to the CNS since they do not cross the blood-brain barrier [32,33]. ASOs bind

161   to their target RNAs through complementary base pairing and can be designed to modify RNA

162   splicing or form an ASO/RNA hybrid that is recognized by RNase H1, leading to cleavage of the

163   target transcript and concomitant reduction in protein expression. Recently, ASOs have shown

164   remarkable efficacy in several animal models of neuron-based CNS disorders and human spinal

165   muscular atrophy patients, the latter leading to the first FDA-approved therapy for this disease [34-

166   44]. Whether ASOs could be delivered to oligodendrocytes *in vivo* and mediate functional

167   improvement in the context of myelin disease was unknown.

168   We tested two separate RNase H ASOs targeting the 5th intron (ASO *Plp1*.a) and 3'UTR

169   (ASO *Plp1*.b) of *Plp1* (Fig. 4a). Administration of ASO *Plp1*.a or ASO *Plp1*.b by

170   intracerebroventricular (ICV) injection robustly reduced *Plp1* expression by 93% and 86% in the

171   cortex and 97% and 94% in the spinal cord of adult wild-type mice, respectively (Extended Data

7

172   Fig. 5a). Both of these *Plp1*-targeting ASOs were well-tolerated based on CNS histology and lack

173   of alteration or reactivity of glial and immune cell markers by qRT-PCR and

174   immunohistochemistry 8 weeks after dosing adult wild-type mice (Extended Data Fig. 5b-f).

175   Administration of ASO *Plp1*.a, ASO *Plp1*.b, or a non-targeting control ASO by ICV

176   injection to male pups after birth revealed widespread distribution and stability of ASOs

177   throughout the neuraxis in both wild-type and *jimpy* mice based on whole-brain

178   immunohistochemical staining at 3 weeks (Fig. 4a, b, and Extended Data Fig. 6a, b). In wild-type

179   mice, *Plp1*-targeting ASOs delivered with this single dose treatment regimen showed robust

180   reductions in *Plp1* transcript by 46-90% and PLP protein by 47-63% across multiple CNS regions,

181   but importantly had no effect on MBP protein levels or overt phenotype (Extended Data Fig. 7a-c

182   and Supplementary Fig. 3). As expected, *jimpy* mice treated with non-targeting control ASO and

183   those left untreated succumbed to their disease at the third postnatal week (Fig. 4c). However,

184   *jimpy* mice treated after birth with a single ICV dose of *Plp1*-targeting ASOs (*Plp1*.a or *Plp1*.b)

185   induced a remarkable extension of lifespan, to our terminal endpoint of 8 months of age (when all

186   animals were processed for histology) (Fig. 4b, c, Supplementary Fig. 3, Supplementary Video 3,

187   and Supplementary Video 4).

188   Treatment with *Plp1*-targeting ASOs increased oligodendrocytes in *jimpy* animals by 3

189   weeks of age, notably in the brainstem, which was sustained through the 8 month terminal end

190   point without additional ASO dosing or other intervention (Fig. 4d-f and Extended Data Fig. 7d,

191   e). Electron micrographs and tissue sections stained with toluidine blue confirmed that some

192   myelinated axons were still present even 8 months post-treatment, but overall myelination was

193   reduced relative to wild-type controls (Fig. 4g, h). Symptomatically, *Plp1*-targeting ASO-treated

194   *jimpy* mice showed only minor PMD pathological phenotypes, including slight tremor and

8

occasional short duration seizures (<15 seconds), but otherwise appeared overtly normal in daily

activities including the ability to breed, which has not previously been achieved by a *jimpy* male

mouse (Supplementary Fig. 3). Rotarod performance of *Plp1*-targeting ASO-treated *jimpy* mice

lagged below wild-type levels, but, strikingly, overall locomotion was restored to wild-type levels

across 2 month, 4 month, and 6 month time points (Fig. 4i, j). Together these data demonstrate that

a single postnatal administration of ASOs elicits a sustained reduction in *Plp1* expression and

dramatically improves myelination, motor performance, and lifespan in a severe point mutation

model of PMD.

In summary, we have shown CRISPR- and ASO-mediated rescue of PMD in the severely

affected *jimpy* mouse model through two independent, technological modalities to achieve mutant

Plp1 suppression. We demonstrate that RNA-based drugs can be used to modulate a disease target

in oligodendrocytes to restore both functional myelin and lifespan in the context of a severe genetic

disorder. These results provide powerful foundational data for the development of clinically

relevant ASO technology to achieve postnatal reduction of *Plp1*. While further pre-clinical

development is needed to optimize the dosing regimen, our results highlight that even a single

ASO treatment can elicit a profound and sustained phenotypic improvement.

The genetic spectrum of PMD patients encompasses hundreds of unique mutations. Our

data nominates a mutation-agnostic approach to collapse this heterogeneity through suppression

of *PLP1*, potentially abrogating the need for per-patient, personalized therapies. Importantly, while

mice display minimal phenotype when *Plp1* is knocked out [13,14,45], *PLP1*-null patients present with

neurological disease, but with considerably later onset, slower progression, and improved clinical

outcomes. While careful titration of normal *PLP1* expression to wild-type levels could be curative

for the majority of patients who harbor gene duplications, reducing mutant *PLP1* in patients with

218   point mutations, while not a full cure, may provide substantial improvement for this disease, which

219   currently has no viable treatment options. Collectively our studies, combined with the feasibility

220   of ASO delivery to the human CNS and current safety data in other CNS indications, support

221   advancement of *PLP1* suppression into the clinic as a disease modifying therapeutic with potential

222   universal applicability to PMD patients. More broadly, our data provide a framework to modulate

223   pathogenic genes or mRNAs in OPCs and oligodendrocytes in order to restore myelination and

224   neurological function in additional genetic and sporadic disorders of myelin.

References:

1   Goldman, S. A., Nedergaard, M. & Windrem, M. S. Glial progenitor cell-based treatment and modeling of neurological disease. *Science* **338**, 491-495, doi:10.1126/science.1218071 (2012).

2   Gupta, N. *et al.* Neural stem cell engraftment and myelination in the human brain. *Sci Transl Med* **4**, 155ra137, doi:10.1126/scitranslmed.3004373 (2012).

3   Saher, G. *et al.* Therapy of Pelizaeus-Merzbacher disease in mice by feeding a cholesterol-enriched diet. *Nat Med* **18**, 1130-1135, doi:10.1038/nm.2833 (2012).

4   Prukop, T. *et al.* Progesterone antagonist therapy in a Pelizaeus-Merzbacher mouse model. *Am J Hum Genet* **94**, 533-546, doi:10.1016/j.ajhg.2014.03.001 (2014).

5   Wishnew, J. *et al.* Umbilical cord blood transplantation to treat Pelizaeus-Merzbacher Disease in 2 young boys. *Pediatrics* **134**, e1451-1457, doi:10.1542/peds.2013-3604 (2014).

6   Tantzer, S., Sperle, K., Kenaley, K., Taube, J. & Hobson, G. M. Morpholino Antisense Oligomers as a Potential Therapeutic Option for the Correction of Alternative Splicing in PMD, SPG2, and HEMS. *Mol Ther Nucleic Acids* **12**, 420-432, doi:10.1016/j.omtn.2018.05.019 (2018).

7   Cailloux, F. *et al.* Genotype-phenotype correlation in inherited brain myelination defects due to proteolipid protein gene mutations. Clinical European Network on Brain Dysmyelinating Disease. *Eur J Hum Genet* **8**, 837-845, doi:10.1038/sj.ejhg.5200537 (2000).

8   Inoue, K. PLP1-related inherited dysmyelinating disorders: Pelizaeus-Merzbacher disease and spastic paraplegia type 2. *Neurogenetics* **6**, 1-16, doi:10.1007/s10048-004-0207-y (2005).

9   Hobson, G. M. & Garbern, J. Y. Pelizaeus-Merzbacher disease, Pelizaeus-Merzbacher-like disease 1, and related hypomyelinating disorders. *Semin Neurol* **32**, 62-67, doi:10.1055/s-0032-1306388 (2012).

10   Nave, K. A., Lai, C., Bloom, F. E. & Milner, R. J. Splice site selection in the proteolipid protein (PLP) gene transcript and primary structure of the DM-20 protein of central nervous system myelin. *Proceedings of the National Academy of Sciences of the United States of America* **84**, 5665-5669 (1987).

11   Garbern, J. Y. Pelizaeus-Merzbacher disease: Genetic and cellular pathogenesis. *Cell Mol Life Sci* **64**, 50-65, doi:10.1007/s00018-006-6182-8 (2007).

12   Baumann, N. & Pham-Dinh, D. Biology of oligodendrocyte and myelin in the mammalian central nervous system. *Physiol Rev* **81**, 871-927 (2001).

13   Griffiths, I. *et al.* Axonal swellings and degeneration in mice lacking the major proteolipid of myelin. *Science* **280**, 1610-1613 (1998).

14   Klugmann, M. *et al.* Assembly of CNS myelin in the absence of proteolipid protein. *Neuron* **18**, 59-70 (1997).

15   Garbern, J. Y. *et al.* Patients lacking the major CNS myelin protein, proteolipid protein 1, develop length-dependent axonal degeneration in the absence of demyelination and inflammation. *Brain* **125**, 551-561 (2002).

16   Hobson, G. M. & Kamholz, J. in *GeneReviews((R))* (eds M. P. Adam *et al.*) (1993).

17   Jinek, M. *et al.* A programmable dual-RNA-guided DNA endonuclease in adaptive bacterial immunity. *Science* **337**, 816-821, doi:10.1126/science.1225829 (2012).

18   Cong, L. *et al.* Multiplex genome engineering using CRISPR/Cas systems. *Science* **339**, 819-823, doi:10.1126/science.1231143 (2013).

19   Dhaunchak, A. S. & Nave, K. A. A common mechanism of PLP/DM20 misfolding causes cysteine-mediated endoplasmic reticulum retention in oligodendrocytes and Pelizaeus-Merzbacher disease. *Proceedings of the National Academy of Sciences of the United States of America* **104**, 17813-17818, doi:10.1073/pnas.0704975104 (2007).

20   Gow, A., Southwood, C. M. & Lazzarini, R. A. Disrupted proteolipid protein trafficking results in oligodendrocyte apoptosis in an animal model of Pelizaeus-Merzbacher disease. *J Cell Biol* **140**, 925-934 (1998).

21   Nevin, Z. S. *et al.* Modeling the Mutational and Phenotypic Landscapes of Pelizaeus-Merzbacher Disease with Human iPSC-Derived Oligodendrocytes. *Am J Hum Genet* **100**, 617-634, doi:10.1016/j.ajhg.2017.03.005 (2017).

22   Elitt, M. S. *et al.* Chemical Screening Identifies Enhancers of Mutant Oligodendrocyte Survival and Unmasks a Distinct Pathological Phase in Pelizaeus-Merzbacher Disease. *Stem Cell Reports* **11**, 711-726, doi:10.1016/j.stemcr.2018.07.015 (2018).

23   Luders, K. A., Patzig, J., Simons, M., Nave, K. A. & Werner, H. B. Genetic dissection of oligodendroglial and neuronal Plp1 function in a novel mouse model of spastic paraplegia type 2. *Glia* **65**, 1762-1776, doi:10.1002/glia.23193 (2017).

24   Miller, M. J., Kangas, C. D. & Macklin, W. B. Neuronal expression of the proteolipid protein gene in the medulla of the mouse. *J Neurosci Res* **87**, 2842-2853, doi:10.1002/jnr.22121 (2009).

25   Lager, A. M. *et al.* Rapid functional genetics of the oligodendrocyte lineage using pluripotent stem cells. *Nat Commun* **9**, 3708, doi:10.1038/s41467-018-06102-7 (2018).

26   Najm, F. J. *et al.* Rapid and robust generation of functional oligodendrocyte progenitor cells from epiblast stem cells. *Nature methods* **8**, 957-962, doi:10.1038/nmeth.1712 (2011).

27   Lee, B. *et al.* Nanoparticle delivery of CRISPR into the brain rescues a mouse model of fragile X syndrome from exaggerated repetitive behaviours. *Nature Biomedical Engineering*, doi:10.1038/s41551-018-0252-8 (2018).

28   Anderson, K. R. *et al.* CRISPR off-target analysis in genetically engineered rats and mice. *Nature methods* **15**, 512-514, doi:10.1038/s41592-018-0011-5 (2018).

29   Tsai, S. Q. & Joung, J. K. Defining and improving the genome-wide specificities of CRISPR-Cas9 nucleases. *Nature reviews. Genetics* **17**, 300-312, doi:10.1038/nrg.2016.28 (2016).

30   Kosicki, M., Tomberg, K. & Bradley, A. Repair of double-strand breaks induced by CRISPR-Cas9 leads to large deletions and complex rearrangements. *Nature biotechnology* **36**, 765-771, doi:10.1038/nbt.4192 (2018).

31   van Overbeek, M. *et al.* DNA Repair Profiling Reveals Nonrandom Outcomes at Cas9-Mediated Breaks. *Molecular cell* **63**, 633-646, doi:10.1016/j.molcel.2016.06.037 (2016).

32   Rinaldi, C. & Wood, M. J. A. Antisense oligonucleotides: the next frontier for treatment of neurological disorders. *Nat Rev Neurol* **14**, 9-21, doi:10.1038/nrneurol.2017.148 (2018).

33   Bennett, C. F., Baker, B. F., Pham, N., Swayze, E. & Geary, R. S. Pharmacology of Antisense Drugs. *Annu Rev Pharmacol Toxicol* **57**, 81-105, doi:10.1146/annurev-pharmtox-010716-104846 (2017).

34   Finkel, R. S. *et al.* Treatment of infantile-onset spinal muscular atrophy with nusinersen: a phase 2, open-label, dose-escalation study. *Lancet* **388**, 3017-3026, doi:10.1016/S0140-6736(16)31408-8 (2016).

35   Hagemann, T. L. *et al.* Antisense suppression of glial fibrillary acidic protein as a treatment for Alexander disease. *Ann Neurol* **83**, 27-39, doi:10.1002/ana.25118 (2018).

36   Finkel, R. S. *et al.* Nusinersen versus Sham Control in Infantile-Onset Spinal Muscular Atrophy. *N Engl J Med* **377**, 1723-1732, doi:10.1056/NEJMoa1702752 (2017).

37   Kordasiewicz, H. B. *et al.* Sustained therapeutic reversal of Huntington's disease by transient repression of huntingtin synthesis. *Neuron* **74**, 1031-1044, doi:10.1016/j.neuron.2012.05.009 (2012).

38   Crooke, S. T., Witztum, J. L., Bennett, C. F. & Baker, B. F. RNA-Targeted Therapeutics. *Cell Metab* **27**, 714-739, doi:10.1016/j.cmet.2018.03.004 (2018).

39   DeVos, S. L. *et al.* Tau reduction prevents neuronal loss and reverses pathological tau deposition and seeding in mice with tauopathy. *Sci Transl Med* **9**, doi:10.1126/scitranslmed.aag0481 (2017).

40   Miller, T. M. *et al.* An antisense oligonucleotide against SOD1 delivered intrathecally for patients with SOD1 familial amyotrophic lateral sclerosis: a phase 1, randomised, first-in-man study. *Lancet Neurol* **12**, 435-442, doi:10.1016/S1474-4422(13)70061-9 (2013).

41   Becker, L. A. *et al.* Therapeutic reduction of ataxin-2 extends lifespan and reduces pathology in TDP-43 mice. *Nature* **544**, 367-371, doi:10.1038/nature22038 (2017).

42   Meng, L. *et al.* Towards a therapy for Angelman syndrome by targeting a long non-coding RNA. *Nature* **518**, 409-412, doi:10.1038/nature13975 (2015).

43   Passini, M. A. *et al.* Antisense oligonucleotides delivered to the mouse CNS ameliorate symptoms of severe spinal muscular atrophy. *Sci Transl Med* **3**, 72ra18, doi:10.1126/scitranslmed.3001777 (2011).

44   Scoles, D. R. *et al.* Antisense oligonucleotide therapy for spinocerebellar ataxia type 2. *Nature* **544**, 362-366, doi:10.1038/nature22044 (2017).

45   Gould, E. A. *et al.* Mild myelin disruption elicits early alteration in behavior and proliferation in the subventricular zone. *eLife* **7**, doi:10.7554/eLife.34783 (2018).

46   Hsu, P. D. *et al.* DNA targeting specificity of RNA-guided Cas9 nucleases. *Nature biotechnology* **31**, 827-832, doi:10.1038/nbt.2647 (2013).

47   Nakagata, N., Okamoto, M., Ueda, O. & Suzuki, H. Positive effect of partial zona-pellucida dissection on the in vitro fertilizing capacity of cryopreserved C57BL/6J transgenic mouse spermatozoa of low motility. *Biol Reprod* **57**, 1050-1055 (1997).

48   Schmid-Burgk, J. L. *et al.* OutKnocker: a web tool for rapid and simple genotyping of designer nuclease edited cell lines. *Genome Res* **24**, 1719-1723, doi:10.1101/gr.176701.114 (2014).

49   Glascock, J. J. *et al.* Delivery of therapeutic agents through intracerebroventricular (ICV) and intravenous (IV) injection in mice. *J Vis Exp*, doi:10.3791/2968 (2011).

Author contributions M.S.E. and P.J.T. conceived and managed the overall study. H.E.S and M.S.E. maintained the animal colonies, tracked survival, and harvested animal tissues. M.S.E. captured video recordings. L.B. and M.S.E. designed and tested sgRNAs. D.F.L., R.A.C., and W.J. performed zygote electroporation and oviduct transfers. H.E.S., B.S.N., K.C.A., and L.B. performed western blotting and protein quantitation. B.E.P, L.B., and K.C.A. performed qRT-PCR. M.M., B.S.N, L.B., H.E.S., and M.S.E. generated the immunohistochemistry data. Y.M. performed optic nerve electrophysiology studies. Y.M., M.H., and H.E.S. processed samples for histology and electron microscopy and analyzed images. M.S.E, K.C.A., B.S.N., and L.B. performed animal behavior. M.S.E., B.S.N., and H.E.O. generated and characterized iPSCs and OPCs in vitro. B.E.P. and F.R. designed and characterized ASOs, tested tolerability in adult mice, recommended the use of ASOs, and contributed to the study design and interpretation of results in the ASO-treated disease model. M.S.E. performed ASO injections in pups. Z.S.N. contributed key components to experimental design, data analysis, and manuscript composition. M.S.E., M.M., L.B., and P.J.T. assembled figures. M.S.E. and P.J.T. wrote the manuscript with input from all authors.

Competing interests P.J.T. is a co-founder and consultant for Convelo Therapeutics, which has licensed patents from CWRU inventors (P.J.T., M.S.E., Z.S.N., and M.M.). P.J.T. and CWRU retain equity in Convelo Therapeutics. P.J.T. is a consultant and on the Scientific Advisory Board of Cell Line Genetics, which performed karyotyping in this study. P.J.T. is Chair of the Scientific Advisory Board (volunteer position) for the Pelizaeus-Merzbacher Disease Foundation. B.E.P. and F.R. are employees of Ionis Pharmaceuticals. No other authors declare competing interests.

Data availability All data generated or analyzed during this study are included in this article and its supplementary information files. Source data for animal survival cohorts in Figs. 1b, 2c, d, and 4c, i, j and are provided in Supplementary Figs. 1 and 3. Raw annotated western blot images for Extended Data Fig. 1d, f and Extended Data Fig. 7b, c, e are provided as Supplementary Figs. 2 and 4. Animals and iPSC lines are available from P.J.T. upon request.

391   **Materials and Methods:**

392   **Mice.** All procedures were in accordance with the National Institutes of Health Guidelines for the

393   Care and Use of Laboratory Animals and were approved by the Case Western Reserve University

394   Institutional Animal Care and Use Committee (IACUC).

395

396   Wildtype (B6CBACa-Aw-J/A) and *jimpy* (B6CBACa-Aw-J/A-Plp1jp EdaTa/J) mice used in this

397   study were purchased from Jackson Laboratory (Bar Harbor, ME). *Jimpy* males exhibit severe

398   neurological phenotypes and die around 3 weeks of age due to mutations in *Plp1* on the X-

399   chromosome.   The colony was maintained by breeding heterozygous females, which lack a

400   phenotype, to wild-type males to generate affected *jimpy* males. Mice were housed under a

401   temperature-controlled environment, 12-h light-dark cycle with ad libitum access to water and

402   rodent chow. All mice were genotyped at ~postnatal day 7 using genomic DNA isolated from tail

403   tips or toes at two loci: 1) the *jimpy* mutation (NM_011123.4:c.623-2A>G) in *Plp1* intron 4, which

404   causes skipping of exon 5 and a truncated PLP protein and 2) the complex indel in *Plp1* exon 3

405   from dual cutting of CRISPR/spCas9 sgRNAs in "CR-*impy*" mice (c.[242_318del; 328_330del]).

406   This "knockdown" causes a frameshift in *Plp1*, a premature stop codon in exon 4, and is predicted

407   to cause nonsense mediated decay of the transcript and loss of protein. Genotyping was performed

408   by standard Sanger sequencing or a custom real time PCR assays (Probe identifiers: Plp1-2 Mut

409   [for *jimpy* mutation in intron 4] and Plp1-5 WT [for CR-*impy* complex deletion in exon 3],

410   Transnetyx, Cordova, TN).

411   Primers for Sanger sequencing included:

412   *jimpy* Forward: AACGCAAAGCAGCACATTTCA

413   *jimpy* Reverse: AGTGCAGCTCTGGGGTTAAT

14

414   CR-*impy* Forward: TCTGTCTGTCCATGCAGGATT

415   CR-*impy* Reverse: GACACACCCGCTCCAAAGAA

416

417   ***Plp1*-targeting sgRNA design.** Mouse *Plp1* sequence was entered into the spCas9 CRISPR

418   sgRNA design tool at crispr.mit.edu [46] and analyzed against the mm10 target genome. *Plp1*-

419   targeting sgRNAs were sorted based on their on-target efficiency while minimizing off-target

420   mutations. On-target nuclease activity was confirmed for each sgRNA using the Guide-it sgRNA

421   Screening Kit (631440, Clontech) according to the manufacturer's instructions. The following

422   sgRNAs were tested, and sgRNAs 3 and 7 were selected for combined use in zygote studies based

423   on localization within the gene, proximity to each other, and ability to target *Plp1*, including its

424   splice isoform *Dm20*:

425   sgRNA1: CCCCTGTTACCGTTGCGCTC

426   sgRNA2: TGGCCACCAGGGAAGCAAAG

427   sgRNA3: AAGACCACCATCTGCGGCAA

428   sgRNA4: GGCCTGAGCGCAACGGTAAC

429   sgRNA5: GCCTGAGCGCAACGGTAACA

430   sgRNA6: TCTACACCACCGGCGCAGTC

431   sgRNA7: CCAGCAGGAGGGCCCCATAA

432   sgRNA8: GAAGGCAATAGACTGACAGG

433

434   **Knockdown of *Plp1* in *jimpy* zygotes using CRISPR-Cas9.** Carrier female oocyte donors were

435   administered 5 IU pregnant mare's serum gonadotropin by intraperitoneal injection (G4877,

436   Sigma-Aldrich), followed by 2.5 IU human chorionic gonadotropin (GC10, Sigma-Aldrich) 48

15

437   hours later. These superovulated females were mated to wild-type males. Zygotes were harvested

438   in FHM medium (MR-025 Sigma-Aldrich) with 0.1% hyaluronidase (H3501, Sigma-Aldrich) and

439   the surrounding cumulus cells were separated. The zona pellucida of each zygote was partially

440   dissected using 0.3M sucrose (S7903, Sigma-Aldrich) in FHM as previously described [47].

441

442   Zygotes were placed in 2x KSOM medium (MR-106, Sigma-Aldrich) with an equal volume

443   of solution containing 100ng/uL sgRNA3, 100ng/uL sgRNA7 (AR01, PNAbio), and 200ng/uL

444   spCas9 mRNA (CR01, PNAbio). Electroporation was performed in a chamber with a 1mm gap

445   between two electrodes using an ECM 830 Square Wave Electroporation System (BTX).

446   Electroporation parameters were set as follows: 32V, 3ms pulse duration, 5 repeats, and 100ms

447   inter-pulse interval. Electroporated zygotes were moved to KSOM medium and then transferred

448   into the oviducts of pseudopregnant females (CD1). Electroporation settings were optimized to

449   achieve maximal cutting efficiency in a separate strain but resulted in a higher rate of embryo loss

450   in our B6CBACa/J strain. Zygotes were electroporated in batches of 54, 56, and 61, which resulted

451   in 4, 3, and 0 pups born. The 7 surviving mice were genotyped after birth and monitored daily for

452   onset of typical *jimpy* phenotypes including tremors, seizures, and early death by postnatal day 21.

453   A founder *jimpy* male with complex deletion containing 80-bp of total deleted sequence in exon 3

454   of *Plp1*, denoted "CR-*impy*" for <u>CR</u>ISPR frameshift-mediated knockdown of *Plp1* in *jimpy*,

455   showed no overt phenotype and was backcrossed for two generations to the wild-type parental

456   strain to reduce potential off-target Cas9 cutting effects (Extended Data Fig. 1b). A colony of mice

457   was bred to evaluate cellular, molecular, and functional phenotypes of contemporaneous isogenic

458   wild-type, *jimpy*, and CR-*impy* male mice. Mice were monitored daily to determine lifespan with

459   statistical significance among groups determined using the log-rank test. Additionally, animals

16

460   surviving beyond 3 weeks were analyzed using behavioral (rotarod and open field testing for motor

461   performance), histology (immunostaining of the CNS for myelin proteins and electron microscopy

462   for myelin ultrastructure), and electrophysiology (conduction velocity of the optic nerve). Details

463   and metadata for all mice in this study including censoring of animals in the survival analysis are

464   found in Supplementary Fig. 1.

465

466   **CRISPR on- and off-target assessment.** CRISPR on- and off-target cutting efficiencies were

467   assessed by high throughput sequencing. PCR primers were designed to encompass each guide on-

468   target site, as well as each top predicted off-target site from the spCas9 CRISPR sgRNA design

469   tool at crispr.mit.edu [46]. Primer sequences were generated using NCBI Primer-BLAST:

PCR amplicon	Genomic Location	Forward Primer	Reverse Primer
sgRNA on-target	*Plp1* exon 3	TCTGTCTGTCCATGCAGGATT	GACACACCCGCTCCAAAGAA
sgRNA3 off-target	Intronic (*Shf,* chr. 2)	TGGGTAGGACAGACAAAGGA	ACAAGGTCATACACACTCAGGC
sgRNA7 off-target	Intergenic (chr. 6)	ACGACCAGACTGCAGATGAAA	TACCCCCAGCACTTGACGAT

470

471   Tails were added to each primer sequence:

472   Forward: TCCCTACACGACGCTCTTCCGATCT

473   Reverse: AGTTCAGACGTGTGCTCTTCCGATCT

474

475   PCR amplification was performed using the KAPA HiFi HotStart ReadyMix (07958935001,

476   Roche) to minimize PCR-based error. Libraries were prepared by adding unique indices by PCR

477   using KAPA HiFi HotStart ReadyMix. All libraries were pooled evenly and quantified using

478   NEBNext® Library Quant Kit for Illumina® (E7630, New England Biolabs) then denatured and

479   diluted per Illumina's MiSeq instructions. 250bp paired-end sequencing was performed using an

17

480   Illumina MiSeq at the Case Western Reserve University School of Medicine Genomics Core

481   Facility. Reads were compared against the consensus sequence and CRISPR-induced indel

482   percentages were determined using the OutKnocker tool at outknocker.org [48].

483

484   **Video recording of mouse phenotypes.** All recording was performed using video recording

485   function on an iPhone (Apple). Videos were color corrected, stabilized, and trimmed to a discrete

486   range using iMovie (Apple). Videos were collated and converted to MP4 format using Adobe After

487   Effects.

488

489   **Immunohistochemistry.** Mice were anesthetized with isoflurane and sacrificed by transcardial

490   perfusion with PBS followed by 4% paraformaldehyde (PFA; 15710, Electron Microscopy

491   Sciences). Tissue was harvested and placed in 4% PFA overnight at 4°C. Samples were rinsed

492   with PBS, equilibrated in 30% sucrose, and frozen in Tissue-Tek® Optimum Cutting Temperature

493   compound (O.C.T.; 25608-930, VWR). Samples were cryosectioned at a 20µm thickness. Sections

494   were washed in phosphate-buffered saline (PBS) and incubated overnight in antibody solution

495   containing 2.5% normal donkey serum (NDS; 017-000-121, Jackson Labs) and 0.25% Triton X-

496   100 (Sigma: T8787). For MBP immunohistochemistry, sections were post fixed in methanol at -

497   20°C for 20 minutes followed by overnight incubation in a PBS based primary antibody solution

498   containing 0.1% Saponin and 2.5% normal donkey serum. Sections were stained using the

499   following antibodies at the indicated concentrations or dilutions: mouse anti-MBP (2µg/mL,

500   808401, Biolegend), rabbit anti-MyRF antibody (1:500; kindly provided by Dr. Michael Wegner),

501   rat anti-PLP (1:500; Lerner Research Institute Hybridoma Core, Cleveland, OH), goat anti-Sox10

502   (0.4µg/mL, AF2864, R&D Systems), rabbit anti-GFAP (1:1000; Z033429-2, Dako), goat anti-

503   IBA1 (0.1mg/mL, ab5076, Abcam), anti-phospho-neurofilament (2ug/ml, 801601, BioLegend),

504   and rabbit anti-ASO (1:2500; Ionis Pharmaceuticals). Secondary immunostaining was performed

505   with Alexa Fluor® antibodies (ThermoFisher) used at 1ug/ml. Nuclei were identified using

506   100ng/ml DAPI (D8417, Sigma). Stained sections were imaged using the Operetta® High Content

507   Imaging and Analysis system (PerkinElmer) and Harmony® software (PerkinElmer) for whole

508   section images and a Leica Sp8 confocal microscope or a Leica DMi8 inverted microscope with

509   Leica Application Suite X software for all other immunohistochemical imaging. To quantify

510   MyRF staining, MyRF+ cells were counted along the length of the whole corpus callosum from

511   medial sagittal sections from three animals per genotype. A one-way ANOVA with correction for

512   multiple comparisons or a Welch's t-test was performed to determine statistical significance across

513   genotypes.

514

515   **qRT-PCR.** Mice were euthanized using isoflurane overdose. Different brain regions (cerebral

516   cortex, cerebellum, and brainstem) were harvested. Each brain region was split in two and half

517   was used for RNA quantification using qRT-PCR, the other for western blot analysis (see below).

518   TRI Reagent (R2050-1-200, Zymo Research) was separately added to tissue and samples were

519   homogenized using Kontes Pellet Pestle Grinders (KT749520-0000, VWR). RNA was extracted

520   using the RNeasy Mini Kit (74104, Qiagen) according to the manufacturer's instructions. Reverse

521   transcription was performed using the iScript cDNA Synthesis Kit (1708891, Biorad) with 1µg of

522   RNA per reaction. Real-Time PCR was then performed on an Applied Biosystems 7300 Real-time

523   PCR system with 10ng cDNA per sample in quadruplicate using Taqman gene expression master

524   mix (4369016, ThermoFisher) and the following pre-designed Taqman gene expression assays

525   (4351370, ThermoFisher): *Plp1* (Mm01297210_m1), *Mbp* (Mm01266402_m1) and *Actb*

19

526   (Mm00607939_s1) (endogenous control). Expression values were normalized to *Actb* and to wild-

527   type samples (for CRISPR cohort) or wild-type untreated samples (for ASO-treated wild-type

528   cohort). Graphpad Prism software was used to perform a one-way ANOVA with Tukey correction

529   or a one-way ANOVA with Dunnett's correction for multiple comparisons to determine statistical

530   significance across genotypes or ASO treatments, respectively.

531

532   **Protein quantification and western blot.** Tissues were obtained as described above. Protein lysis

533   buffer consisting of RIPA buffer (R0278, Sigma), cOmplete™ Mini EDTA-free Protease Inhibitor

534   Cocktail (11836170001, Sigma), Phosphatase Inhibitor Cocktail 3 (P0044, Sigma), Phosphatase

535   Inhibitor Cocktail 2 (P5726, Sigma), and BGP-15 (B4813, Sigma) was added to each sample.

536   Tissue was homogenized using Dounce Tissue Grinders (D8938, Sigma). Lysate was separated by

537   centrifugation at 17000g for 15 minutes at 4°C. A BCA standard curve was generated using the

538   Pierce BCA Protein Assay Kit (23225, Thermo Scientific) and used to samples to an equivalent

539   protein concentration. Equal amounts of sample were run on a NuPAGE 4-12% Bis-Tris Protein

540   gel (NP0335BOX or NP0329BOX, Thermo Fisher), then electrophoretically transferred to a

541   PVDF membrane (LC2002, Invitrogen or 926-31097, Li-Cor). The membrane was blocked with

542   5% milk in TBS-T for an hour, then hybridized with mouse anti-MBP antibody (1µg/mL; 808401,

543   Biolegend) or rat anti-PLP antibody (1:1000; Lerner Research Institute Hybridoma Core,

544   Cleveland, OH) overnight at 4°C. Blots were then washed in TBS-T and incubated in goat anti-

545   mouse HRP (1:2500, 7076, Cell Signaling), goat anti-rat HRP (1:2500, 7077, Cell Signaling), or

546   IRDye secondaries (1:20000, 925, Li-Cor). Each sample was normalized to B-actin using HRP-

547   conjugated mouse anti-B-actin (1:10000, A3854-200UL, Sigma-Aldrich). All secondary

548   antibodies were incubated for one hour at room temperature. Blots were analyzed with the

20

549   Odyssey® Fc imaging system (Li-Cor). Graphpad Prism software was used to perform a one-way

550   ANOVA with Tukey correction or a one-way ANOVA with Dunnett's correction for multiple

551   comparisons to determine statistical significance across genotypes or ASO treatments,

552   respectively. Raw annotated images of full western blots are provided in Supplementary Figs. 2

553   and 4.

554

555   **Electron microscopy and toluidine blue staining.** Mice were anesthetized with isoflurane and

556   rapidly euthanized. Tissue was collected after transcardial perfusion with PBS followed by 4%

557   paraformaldehyde and 2% glutaraldehyde (16216, Electron Microscopy Sciences) in 0.1M sodium

558   cacodylate buffer, pH 7.4 (11652, Electron Microscopy Sciences), except for 6 month optic nerve

559   samples which were placed directly into fixative without perfusion. Samples were post-fixed with

560   1% osmium tetroxide (19150, Electron Microscopy Sciences) and stained with 0.25% uranyl

561   acetate (22400, Electron Microscopy Sciences), en bloc. Samples were dehydrated using

562   increasing concentrations of ethanol, passed through propylene oxide, and embedded in Eponate

563   12™ epoxy resin (18012, Ted Pella). Silver–colored sections were prepared (Leica EM UC6),

564   placed on 300 mesh nickel grids (T300-Ni, Electron Microscopy Sciences), stained with 2% uranyl

565   acetate in 50 % methanol, and stained with lead citrate (17800, Electron Microscopy Sciences).

566   Sections were imaged using a FEI Tecnai Spirit electron microscope at 80 kV. Myelinated axons

567   were manually counted from the sections made on the middle part of the nerve lengthwise and at

568   least three areas across the optic nerve diameter using Adobe Photoshop (Adobe Systems).

569   Graphpad Prism software was used to perform a one-way ANOVA with Tukey correction to

570   determine significance across genotypes. Toluidine Blue (22050, Electron Microscopy Sciences)

571   stained 1μm sections were prepared from same epoxy resin embedded samples above and

21

572   visualized with a light microscope (Zeiss Axioskop2) using plan-NEOFLUAR 100X 1.30 oil

573   objective lens and images were captured using a Scion 1394 color camera with ImageJ software.

574

575   **Optic nerve electrophysiology.** Mice were deeply anesthetized with isoflurane and euthanized.

576   Each eye with its attached optic nerve was dissected and placed in Ringer's solution consisting of

577   129mM NaCl (BP358-212, Fisher Scientific), 3mM KCl (BP366-500, Fisher Scientific), 1.2mM

578   NaH_2PO_4 (1-3818, J. T. Baker Chemical), 2.4mM $CaCl_2$ (C79-500, Fisher Scientific), 1.3mM

579     $MgSO_4$ (M2643, Sigma), 20mM $NaHCO_3$ (S233-500, Fisher Scientific), 3mM HEPES (H3375,

580   Sigma), 10mM glucose (G5767, Sigma), oxygenated using a 95%O_2/5% CO_2 gas mixture. Each

581   nerve was carefully cleaned, transected behind the eye, at the optic chiasm, and allowed to recover

582   for one hour in oxygenated Ringer's solution at room temperature (22–24°C). Each end of the

583   nerve was set in suction electrodes, pulled from polyethylene tubing (PE-190, BD Biosciences).

584   Monophasic electrical stimuli were applied to the proximal end of the nerve and recordings were

585   captured at the distal end. The recovery of the response was monitored every 20 min for one hour,

586   and only fully recovered samples were subjected to additional stimuli. Stimuli were generated with

587   a S48 stimulator (Grass Technologies) and isolated from ground with PSIU6B unit (Grass

588   Technologies). Supra-threshold stimulus was determined using 30µs stimulus duration. The

589   response was amplified 100X with P15D preamplifier (Grass Technologies), monitored with

590   oscilloscope (V1585, Hitachi), digitized with Digidata1550A (Axon Instruments) and recorded

591   using 50kHz sampling rate with AxoScope software (Axon Instruments). The distance between

592   the electrodes was measured and used to calculate the conduction velocity of the compound action

593   potential (CAP) peaks at their latency. Recorded signals were analyzed using AxoScope software.

594

Open Field Testing. Locomotion was assessed by open field testing. Animals were placed in the center of a 20-inch by 20-inch square box and all movements were captured for a total of five minutes using ANY-maze software version 5.0 (Stoelting Co). Total distance traveled was reported for each animal. Graphpad Prism software was used to perform a one-way ANOVA with Tukey correction or a one-way ANOVA with Dunnett's correction for multiple comparisons to determine statistical significance across genotypes or ASO treatments, respectively.

Rotarod Testing. Motor performance was assessed using a Rota Rod Rotomax 5 (Columbus Instruments) with a 3cm diameter rotating rod. Immediately prior to testing animals were trained at a constant speed of 4 rounds per minute (rpm) for a total of two minutes. Testing began at 4 rpm with an acceleration of 0.1 rpm/s. Time to fall was recorded from three independent trials, and the average value for each animal was reported. Between training and each experimental trial animals were allowed to rest for at least five minutes. Graphpad Prism software was used to perform a one-way ANOVA with Tukey correction or a one-way ANOVA with Dunnett's correction for multiple comparisons to determine statistical significance across genotypes or ASO treatments, respectively.

Generation of iPSCs. Tail tips (2 mm piece from 8 day old CR-*impy* mice) were bisected, placed on Nunclon-Δ 12-well plates (150628, ThermoFisher), and covered with a circular glass coverslip (12-545-102; Fisher Scientific) to maintain tissue contact with the plate and enable fibroblast outgrowth. Tail-tip fibroblasts were cultured in 'fibroblast medium' consisting of DMEM (11960069, ThermoFisher) with 10% fetal bovine serum (FBS; 16000044, ThermoFisher), 1x non-essential amino acids (11140050, ThermoFisher), 1x Glutamax (35050061, ThermoFisher), and

23

0.1 mM 2-mercaptoethanol (M3148, Sigma Aldrich) supplemented with 100U/mL penicillin-streptomycin (15070-063, ThermoFisher). Medium was changed every day for the first 3 days and then every other day.

Fibroblasts were seeded at approximately 1.4×10^4 cells/cm^2 on Nunclon-Δ dishes in fibroblast medium, and allowed to equilibrate overnight. The following day medium was removed and replaced with an equal volume of pHAGE2-TetOminiCMV-STEMCCA-W-loxp lentivirus encoding a floxed, doxycycline-inducible polycistronic Oct4, Sox2, Klf4, and c-Myc construct and pLVX-Tet-On-Puro (632162, Clontech) lentivirus supplemented with 8µg/mL polybrene (107689, Sigma). Lentivirus was prepared using the Lenti-X Packaging Single Shots (631275, Clontech) according to manufacturer's instructions. Three hours later lentivirus medium was removed and replaced with fibroblast medium supplemented with 2 µg/ml doxycycline (631311, Clontech). The following day media was removed and replaced with an equal volume of pHAGE2-TetOminiCMV-STEMCCA-Wloxp and pLVX-Tet-On-Puro lentivirus supplemented with 8µg/mL polybrene. Three hours later lentivirus media was diluted 1:2 with fibroblast medium. Medium was changed each day with fibroblast medium supplemented with 2 µg/ml doxycycline and 10^3 units/ml LIF. After 3 days fibroblasts were lifted using Accutase and seeded on Nunclon-Δ plates, atop a feeder layer of irradiated mouse embryonic fibroblasts (iMEFs; produced in-house) previously plated at 1.7×10^4 cells/cm^2 on 0.1% gelatin (1890, Sigma) coated Nunclon-Δ plates in "pluripotency medium" consisting of Knockout DMEM (10829-018, ThermoFisher), 5% FBS, 15% knockout replacement serum (10828028, ThermoFisher), 1x Glutamax, 1x nonessential amino acids, 0.1 mM 2-mercaptoethanol, and 10^3 units/ml LIF (LIF; ESG1107, EMD Millipore) supplemented with 2 µg/ml doxycycline. Medium was changed every day until iPSC colonies

641   began to emerge. Individual colonies were picked and dissociated in accutase and were

642   individually plated in single wells of Nunclon-Δ 12-well plates, atop an iMEF feeder layer in

643   pluripotency medium supplemented with 2 µg/ml doxycycline. Clones were further expanded,

644   with daily medium changes. iPSC colonies were stained for pluripotency markers and karyotyped

645   at the seventh passage after derivation (Cell Line Genetics; Madison, WI). CR-*impy* iPSCs were

646   derived and characterized for this study (line identifier jpCR100.1). Isogenic comparator *jimpy*

647   (line identifier i.jp-1.6) and wild-type (line identifier i.wt-1.0) iPSC lines were described and

648   characterized separately [22]. Genotypes of iPSCs were re-verified prior to use.

649

650   **Generation of iPSC-derived OPCs.** iPSCs were differentiated to OPCs as previously described

651   [25,26]. In brief, iPSC were isolated from their iMEF feeder layer using 1.5mg/mL collagenase type

652   IV (17104019, ThermoFisher) and dissociated with either 0.25% Typsin-EDTA or Accutase and

653   seeded at 7.8×10^4 cells/cm2 on Costar Ultra-Low attachment 6-well plates (3471, Corning).

654   Cultures were then directed through a stepwise differentiation process to generate pure populations

655   of OPCs. OPCs were maintained in "OPC medium" consisting of DMEM/F12 (11320082,

656   ThermoFisher), 1x N2 supplement (AR009, R&D Systems), 1x B-27 without vitamin A

657   supplement (12587-010, ThermoFisher), and 1x Glutamax (collectively "N2B27 medium"),

658   supplemented with 20 ng/mL fibroblast growth factor 2 (FGF2; 233-FB, R&D Systems) and 20

659   ng/mL platelet-derived growth factor-AA (PDGF-AA; 221-AA, R&D Systems). Medium was

660   changed every other day. For characterization of purity, iPSC-derived OPCs from all genotypes

661   were fixed with 4% PFA and immunostained for canonical OPC transcription factors, Olig2 and

662   Sox10.

663

In vitro **assessment of oligodendrocyte differentiation and survival from OPCs.** OPCs from each genotype were plated in parallel onto Nunclon-Δ 96-well plates (150628, ThermoFisher) that were first coated with 100 µg/mL poly(L-ornithine) (P3655, Sigma), followed by 10 µg/ml laminin solution (L2020, Sigma). For the oligodendrocyte differentiation assay, 25,000 cells were seeded per well in media that consisted of DMEM/F12 (11320082, ThermoFisher), 1x N2 supplement (AR009, R&D Systems), 1x B-27 without vitamin A supplement (12587-010, ThermoFisher), and 1x Glutamax, supplemented with T3 (40ng/ml), Noggin (100ng/ml), cAMP (10uM), IGF (100ng/ml) and NT3 (10ng/ml). All plates were incubated at 37°C and 5% CO_2 for 3 days. Cells were immunostained using for myelin protein markers. Eight fields were captured per well and the total number of MBP+ cells were quantified for each cell line. Graphpad Prism software was used to perform a one-way ANOVA with Tukey correction for multiple comparisons to determine statistical significance across genotypes.

Immunocytochemistry. Cells were fixed with 4% paraformaldehyde (PFA) in phosphate buffered saline (PBS). After fixation, cells were permeabilized with 0.2% Triton X-100 in PBS followed by blocking in 10% donkey serum in PBS. Cells were stained overnight at 4°C with the following primary antibodies diluted in blocking solution: rat anti-MBP (1:100; ab7349, Abcam), rat anti-PLP (1:5000; Lerner Research Institute Hybridoma Core, Cleveland, OH), goat anti-Sox10 (2µg/mL; AF2864, R&D Systems), rabbit anti-Olig2 (1:1000; 13999-1-AP, ProteinTech), rabbit anti-Nanog (0.4µg/mL; AB21624, Abcam), mouse anti-Oct4 (0.4µg/mL; SC-5279, Santa Cruz). For secondary immunostaining, Alexa Fluor® antibodies (ThermoFisher) were used at 1ug/ml, and DAPI (100ng/mL, D8417, Sigma) was used at to identify nuclei.

687   **ASO design and characterization.** Second generation ASOs were designed to target mouse *Plp1*.

688   ASOs consisted of 20-mer nucleotide sequences with 2′-O-methoxyethyl (MOE) modifications

689   and a mixed backbone of phosphorothioate and phosphodiester internucelotide linkages.

690

691   ASOs were screened for efficacy in primary E16 cortical cultures, as previously described [35].

692   Briefly, cells were treated with ASOs at 37°C/5% CO_2 for 3 days, RNA was isolated, and *Plp1*

693   transcript level was quantified with qRT-PCR on Step One instruments (Thermo Fisher). *Plp1*

694   mRNA was normalized to total RNA measured with the Quant-iTTM RiboGreen® RNA reagent.

695   ASOs that efficiently reduced *Plpl* mRNA were selected for *in vivo* screening and tolerability

696   studies.

697

698   Lead ASOs were administered to 8 week old C57BL/6J mice (Jackson Labs) via single 500 μg

699   intracerebroventricular (ICV) injection and *Plp1* mRNA levels were measured by RT-qPCR in

700   cortex and spinal cord tissue after 2 weeks. ASOs with greater than 90% *Plp1* mRNA reduction

701   were selected for further characterization. These were administered to mice via single 300 μg ICV

702   bolus injection to test for efficacy and tolerability, as measured by markers of glial cell activation,

703   8 weeks post-ICV. Levels of *Plp1* mRNA as well as markers of astro- or micro-glial activation,

704   *Gfap*, *Aif1*, and *CD68*, were assessed by RT-qPCR using the following custom primer/probe sets

705   (Integrated DNA Technologies):

Gene	Forward primer	Reverse primer	Probe (5'FAM; 3'TAMRA)
Plp1	CTGATGCCAGAATGTATGGTGT	AGGTGGAAGGTCATTTGGAAC	TGCAGATGGACAGAAGGTTGGAGC
Gfap	GAAACCAGCCTGGACACCAA	TCCACAGTCTTTACCACGATGTTC	TCCGTGTCAGAAGGCCACCTCAAGA
Aif1	TGGTCCCCCAGCCAAGA	CCCACCGTGTGACATCCA	AGCTATCTCCGAGCTGCCCTGATTGG
Cd68	TGGCGGTGGAATACAATGTG	GATGAATTCTGCGCCATGAA	CCTCCCACAGGCAGCACAGTGG

706

27

707   Immunohistochemical staining was used to assess morphology of astrocytes (rabbit polyclonal

708   antibody, DAKO) and microglia (rabbit polyclonal antibody, WAKO) in formalin-fixed, paraffin

709   embedded brain and spinal cord sections. *Plp1* ASO.a (intron 5) and ASO.b (3' UTR) were

710   selected for use in j*impy* mice, as well as a control ASO with no known murine target.

711

712   **Therapeutic application of ASOs to postnatal mice.** Male pups from crosses between *jimpy*

713   mutation carrier females and wild-type males were administered 30ug of either *Plp1*-targeting

714   ASOs *Plp1*.a, *Plp1*.b, a control non-targeting ASO, or left untreated. ASOs were administered

715   using a Hamilton 1700 gastight syringe (7653-01, Hamilton Company) by ICV injection to

716   cryoanesthetized mice. The needle was placed between bregma and the eye, 2/5 the distance from

717   bregma, and inserted to a depth of 2mm according to published protocols [49]. A total volume of 2uL

718   was administered to the left ventricle. Mice were allowed to recover on a heating pad and

719   subsequently reintroduced to the mother.

720

721   Mice were genotyped at approximately postnatal day 7 and monitored daily for onset of typical

722   *jimpy* phenotypes including tremors, seizures, and early death by 3 weeks of age. Lifespan was

723   determined for each animal with statistical significance among groups determined using the log-

724   rank test. All mice surviving to a pre-determined endpoint of 8 months of age were sacrificed for

725   histological analysis. Additionally, animals surviving beyond 3 weeks were analyzed using

726   behavioral (rotarod and open field testing for motor performance). Details and metadata for all

727   mice in this study are found in Supplementary Fig. 3.
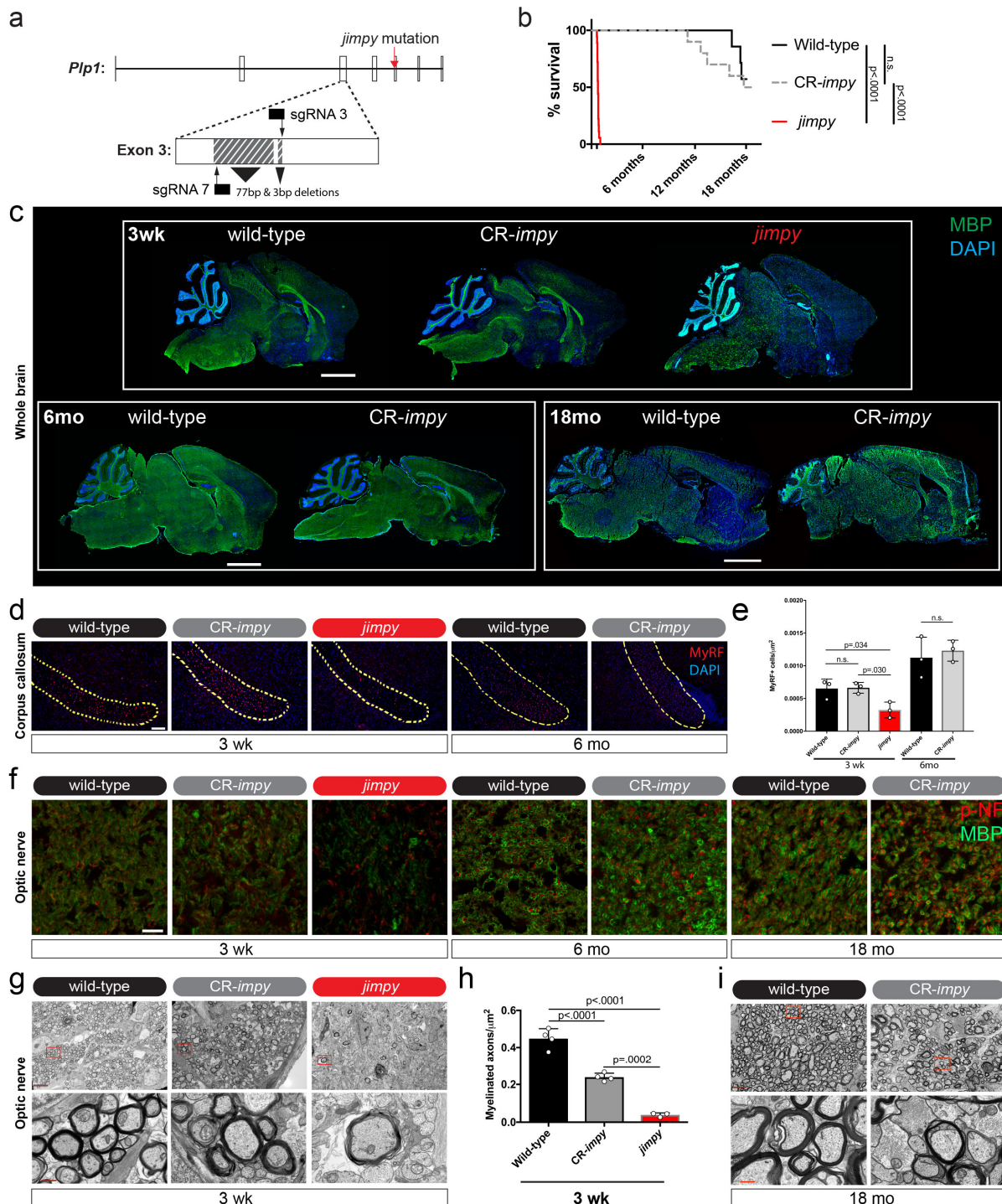
728 **FIGURE 1**

729

732 **Fig. 1 | Prevention of PMD and rescue of lifespan by CRISPR-mediated knockdown of *Plp1***
733 **in the germline of *jimpy* mice.**
734 **a,** Schematic of *Plp1* targeting in *jimpy* using CRISPR-spCas9. The location of the *jimpy* mutation
735 in the 3' splice acceptor site of intron 4 is indicated by a red arrow. Two separate sgRNAs (denoted

29

736 3 and 7) were utilized and their DNA binding sites are indicated by solid black bars and their
737 predicted cutting sites by black arrows. The complex, frameshift deletion of 80 base-pairs of
738 deleted sequence within exon 3 in the CR-*impy* mice is shown by two grey hashed boxes (see
739 Extended Data Fig. 1 for more detail and sequence traces).

740 **b,** Kaplan-Meier plot comparing lifespan of contemporaneous wild-type, *jimpy,* and CR-*impy*
741 mouse cohorts. n = 25, 18, and 23 starting animals in the wild-type, *jimpy*, and CR-*impy* cohorts,
742 respectively (see Supplementary Fig. 1 for metadata of every animal in this study including
743 censoring of animals for molecular and functional studies at pre-determined time points). p-values
744 calculated using the log-rank test between cohorts.

745 **c,** Representative immunohistochemical images of whole-brain sagittal sections showing MBP+
746 oligodendrocytes (green) and total DAPI+ cells (blue) in wild-type, CR-*impy*, and *jimpy* mice at 3
747 weeks, 6 months, and 18 months of age. Scale bar, 2mm.

748 **d,** Representative sagittal immunohistochemical images of the rostral end of the corpus collosum
749 showing MyRF+ oligodendrocytes (red) and total DAPI+ cells (blue) in wild-type, CR-*impy*, and
750 *jimpy* mice at 3 weeks, 6 months, and 18 months of age. Scale bar, 100μm.

751 **e,** Quantification of MyRF+ oligodendrocytes in the corpus callosum at 3 weeks and 6 months of
752 age for each genotype. n=3 mice per genotype at each time point. Error bars show mean ± standard
753 deviation. p-values calculated using ANOVA with Tukey correction for multiple comparisons at
754 3 weeks and Welch's t-test at 6 months.

755 **f,** Representative confocal immunohistochemical images of optic nerve cross sections showing
756 MBP+ oligodendrocytes (green) and phospho-neurofilament+ intact axons (red) in wild-type, CR-
757 *impy*, and *jimpy* mice at 3 weeks, 6 months, and 18 months of age. Scale bar, 20μm.

758 **g,** Representative electron micrograph images showing myelination in optic nerve cross sections
759 in wild-type, CR-*impy*, and *jimpy* mice at 3 weeks of age. Lower panel is a higher magnification
760 of red boxed area in the upper panel. Upper panel scale bar, 5μm and lower panel scale bar is
761 0.5μm.

762 **h,** Quantification of the number of myelinated axons in optic nerves of each genotype at postnatal
763 week 3. n=4 mice for wild-type and CR-*impy* and n=3 mice for and *jimpy* genotypes. Error bars
764 show mean ± standard deviation. p-values calculated using ANOVA with Tukey correction for
765 multiple comparisons.

766 **i,** Representative electron micrograph images of myelination in optic nerve cross sections in wild-
767 type and CR-*impy* mice at 18 months of age. Lower panel is a higher magnification of red boxed
768 area in the upper panel. Upper panel scale bar, 5μm and lower panel scale bar is 0.5μm.

FIGURE 2
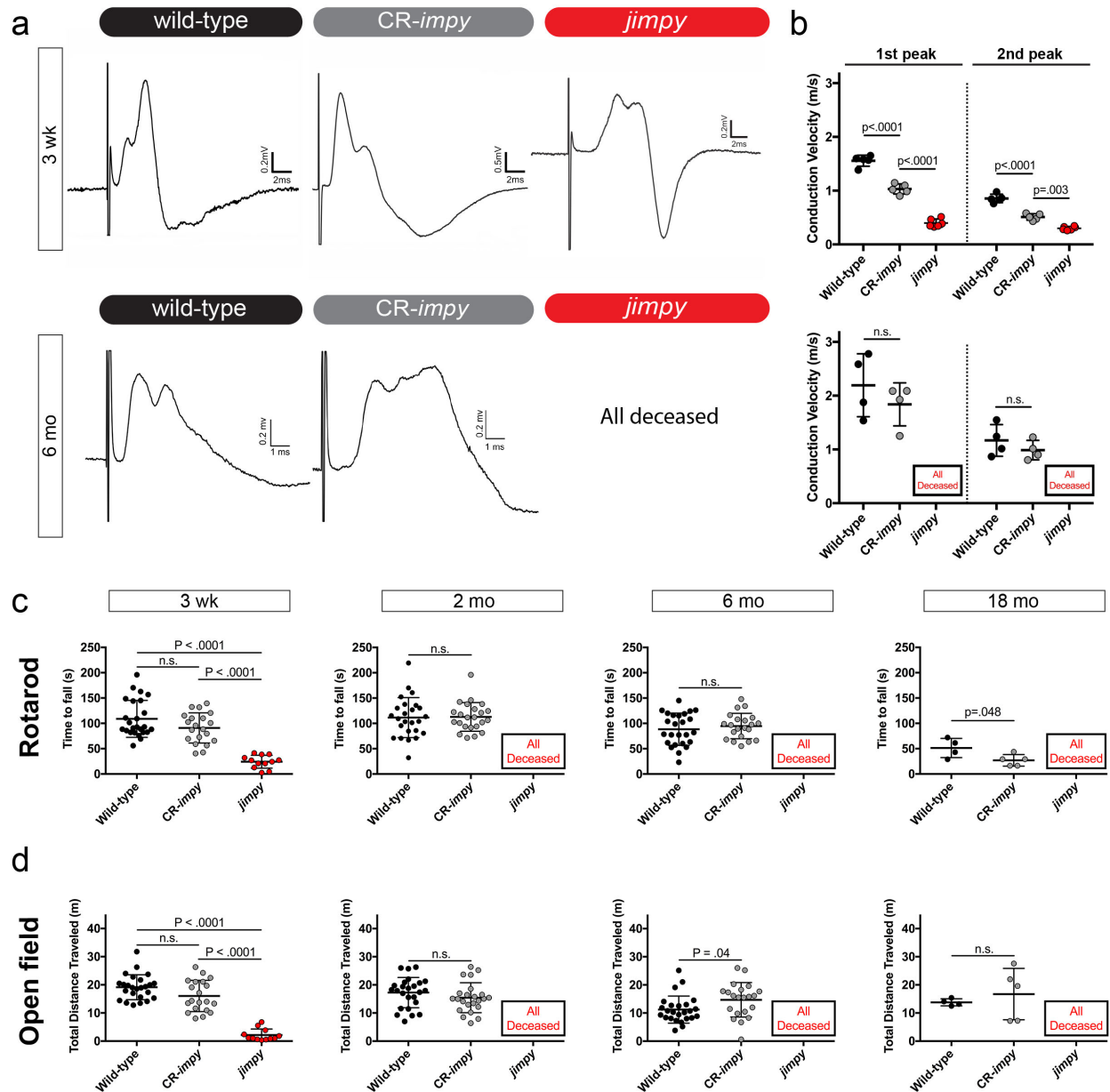
Fig. 2 | CRISPR-mediated knockdown of *Plp1* in *jimpy* mice restores myelin function and motor phenotypes.

 a, Representative electrophysiology optic nerve conduction traces from wild-type, CR-*impy*, *jimpy* mice at 3 weeks and 6 months of age.

b, Quantification of optic nerve conduction velocities from wild-type, CR-*impy*, *jimpy* mice at 3 weeks and 6 months of age. Each point represents an individual biological replicate (optic nerves from separate mice) with n = 5, 5, and 6 wild-type, *jimpy*, and CR-*impy* mice, respectively, at the 3 week time point and n = 4 wild-type and CR-*impy* mice each at the 6 month time point. Error bars show mean ± standard deviation. p-values calculated using one-way ANOVA with Tukey

31

782   correction for multiple comparisons at 3 weeks and two-way, unpaired t-test at 6 months.
783   **c,** Comparison of motor function and coordination of wild-type, CR-*impy*, and *jimpy* mice at 3
784   weeks (n=25, 20, and 12 wild-type, *jimpy*, and CR-*impy* mice), 2 months (n= 25 and 23 wild-type
785   and CR-*impy* mice), 6 months (n=25 and 21 wild-type and CR-*impy* mice), and 18 months of age
786   (n=4 and 5 wild-type and CR-*impy* mice) by accelerating rotarod performance. Individual data
787   points represent the mean time to fall of three separate trials for each biological replicate (separate
788   mice). Error bars show mean ± standard deviation. p-values calculated using one-way ANOVA
789   with Tukey correction for multiple comparisons at 3 weeks or two-way, unpaired t-test at later
790   time points. See Supplementary Fig. 1 for raw data values.
791   **d,** Comparison of locomotor activity of wild-type, CR-*impy*, and *jimpy* mice at 3 weeks (n=25, 20,
792   and 12 wild-type, *jimpy*, and CR-*impy* mice), 2 months (n= 25 and 23 wild-type and CR-*impy*
793   mice), 6 months (n=25 and 21 wild-type and CR-*impy* mice), and 18 months of age (n=4 and 5
794   wild-type and CR-*impy* mice) by open field testing. Individual data points represent total distance
795   traveled for each biological replicate (separate mice). Error bars show mean ± standard deviation.
796   p-values calculated using one-way ANOVA with Tukey correction for multiple comparisons at 3
797   weeks or two-way, unpaired t-test at later time points. See Supplementary Fig. 1 for raw data
798   values.
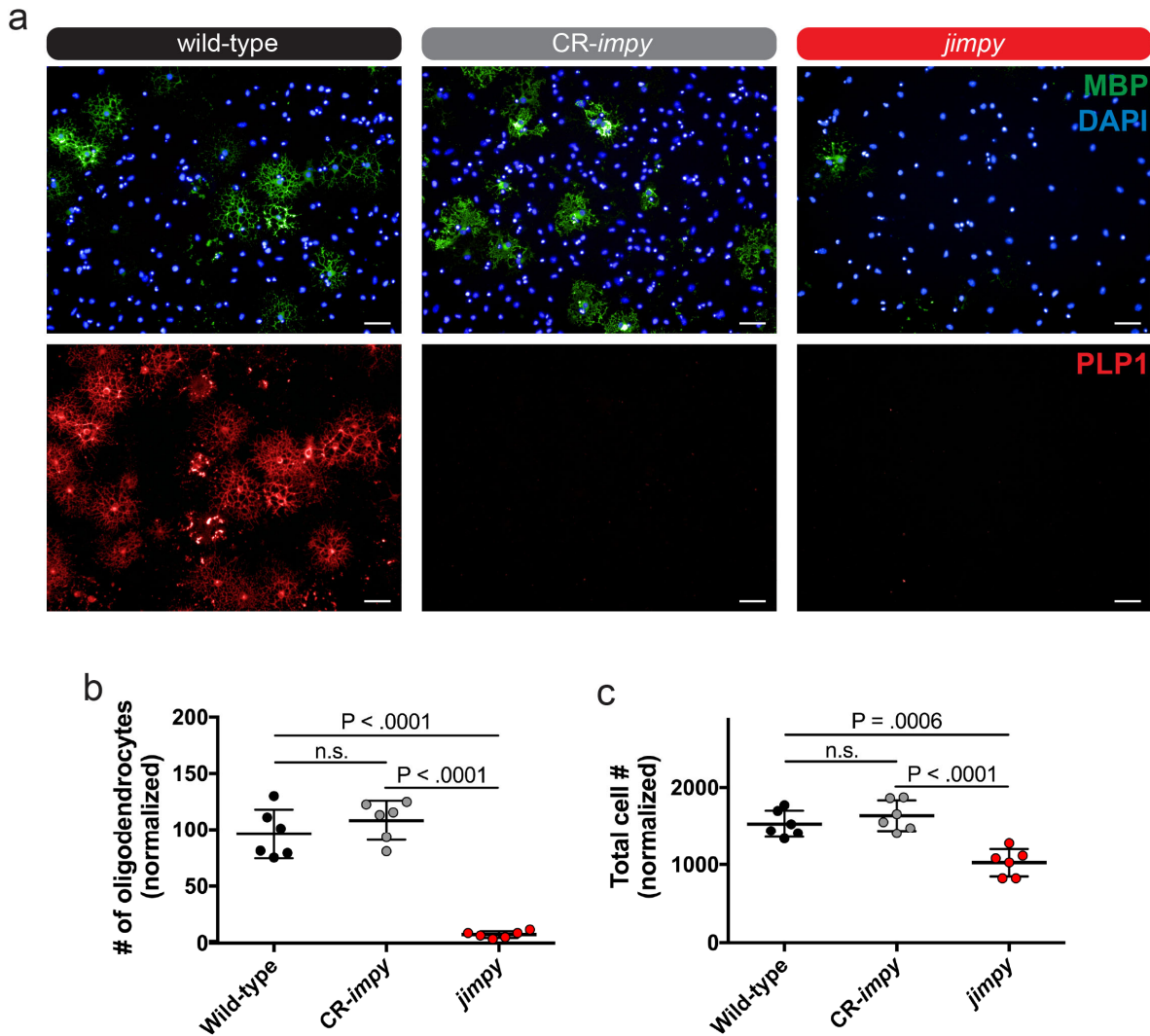
FIGURE 3

Fig. 3 | CRISPR-mediated knockdown of *Plp1* in *jimpy* OPCs rescues survival of differentiating oligodendrocytes *in vitro*.

a, Representative immunocytochemistry images of MBP+ oligodendrocytes and PLP+ oligodendrocytes from wild-type, CR-*impy*, and *jimpy* iPSC-derived OPCs differentiated *in vitro* for 3 days. Top and bottom rows are the same field but channels are separated for clarity. Note the PLP1 antibody detects a C-terminal peptide sequence not present in jimpy and therefore absence of staining simply serves as validation of jimpy genotype but not quantification of total PLP1 protein (for which there are no validated N-terminal antibodies for immunostaining). Scale bar, 50μm.

b-c, Quantification of MBP+ oligodendrocytes (b) and total DAPI+ cells (c). Error bars show mean ± standard deviation. n=6 technical replicates (single cell line per genotype with 6 separate wells scored). p-values calculated using one-way ANOVA with Tukey correction for multiple comparisons.
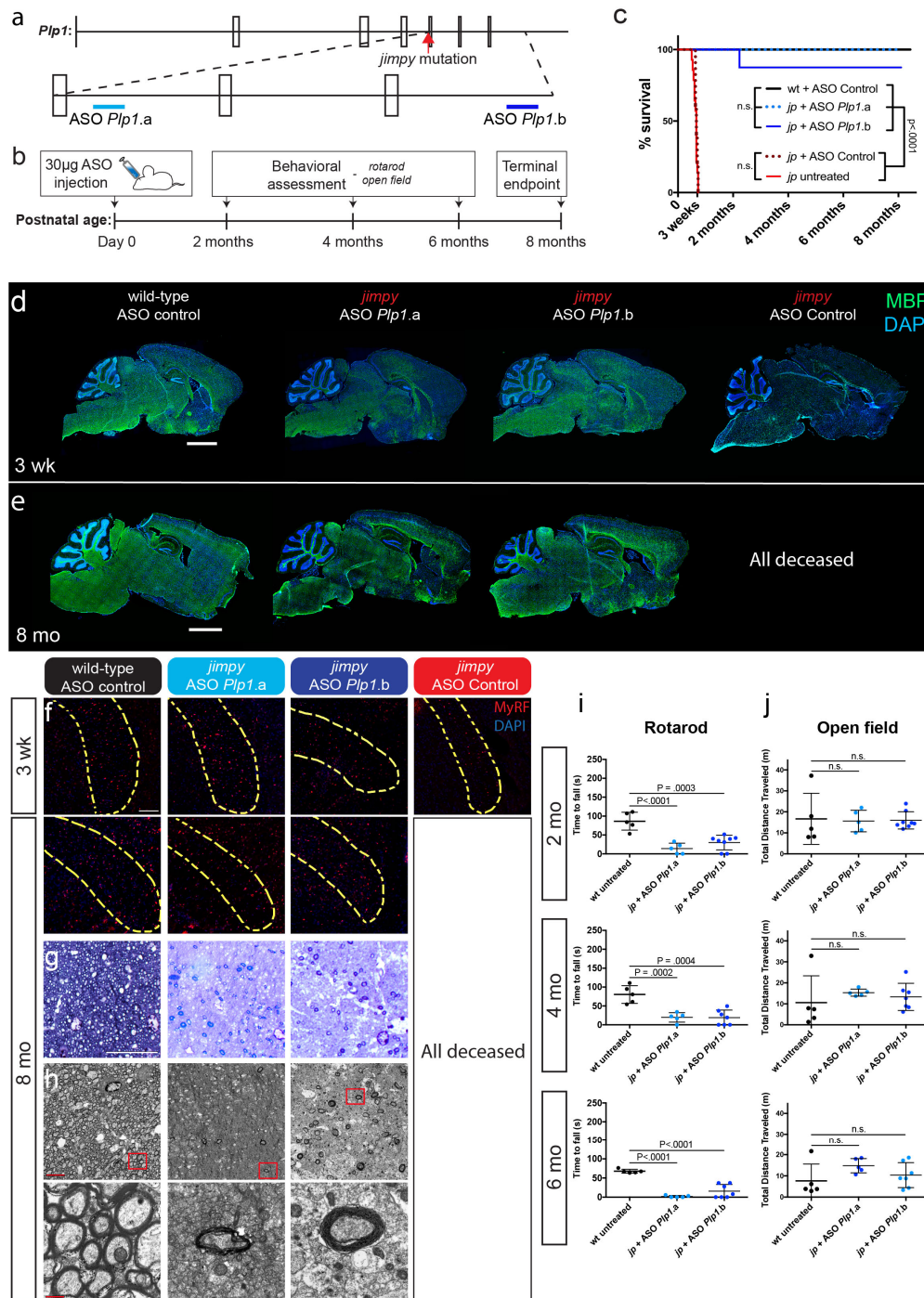
FIGURE 4

Fig. 4 | Postnatal delivery of *Plp1*-targeted antisense oligonucleotides rescues lifespan and partially restores functional myelinating oligodendrocytes in *jimpy* mice.

a, Schematic of the binding location of the two independent ASOs within intron 5 and the 3' UTR of the *Plp1* pre-mRNA. The location of the *jimpy* mutation in the 3' splice acceptor site of intron 4 is indicated by a red arrow.

b, Schematic of the experimental design for ASO experiments. A single 30ug dose of ASO was administered by intracerebroventricular injection into the lateral ventricle within one day after birth. Functional assessment was performed at 2, 4, and 6 months of age and the experiment was terminated for histological analyses at 8 months of age.

c, Kaplan-Meier plot depicting the survival of *jimpy* mice treated with two independent *Plp1*-targeting ASOs compared to controls. Groups included: untreated wild-type (n=5), wild-type treated with ASO-control (n=12), untreated *jimpy* (n=14), *jimpy* treated with ASO-control (n=5), *jimpy* treated with ASO-*Plp1*.a (n=5), and *jimpy* treated with ASO-*Plp1*.b (n=8). See Supplementary Fig. 3 for metadata of every animal in this study including behavioral studies at pre-determined time points. p-values calculated using the log-rank test.

d-e, Representative immunohistochemical images of 3 week (d) and 8 month (e) whole-brain sagittal sections showing MBP+ oligodendrocytes (green) and total DAPI+ cells (blue) in control and *jimpy* mice treated with indicated ASOs. Scale bar, 2mm.

f, Representative sagittal images of the 3 week old rostral corpus callosum showing MyRF+ oligodendrocytes in control and *jimpy* mice treated with indicated ASOs. Scale bar, 100um.

g, Representative toluidine blue stained images showing myelinated axons in the corpus callosum of 8 month old wild-type and *jimpy* mice treated with the indicated ASOs. Scale bar, 20um.

h, Representative electron micrograph images showing myelination in the corpus callosum of 8 month old wild-type and *jimpy* animals treated with the indicated ASOs. Lower panel is a higher magnification of red boxed area in the corresponding image in the upper panel. Upper panel scale bar, 5um and lower panel scale bar is 0.5um.

i, Comparison of motor function and coordination of 2 month (n=5, 5, and 8 for untreated wild-type, ASO-*Plp1*.a-treated *jimpy*, and ASO-*Plp1*.b-treated *jimpy* mice), 4 month (n=5, 5, and 7 for untreated wild-type, ASO-*Plp1*.a-treated *jimpy*, and ASO-*Plp1*.b-treated *jimpy* mice), and 6 month (n=5, 5, and 7 for untreated wild-type, ASO-*Plp1*.a-treated *jimpy*, and ASO-*Plp1*.b-treated *jimpy* mice) old mice by accelerating rotarod performance. Individual data points represent the mean time to fall of three separate trials for each biological replicate (separate mice). Error bars show mean ± standard deviation. p-values calculated using one-way ANOVA with Dunnett's correction for multiple comparisons. See Supplementary Fig. 3 for raw data values.

j, Comparison of locomotor activity of 2 month (n=5, 5, and 8 for untreated wild-type, ASO-*Plp1*.a-treated *jimpy*, and ASO-*Plp1*.b-treated *jimpy* mice), 4 month (n=5, 5, and 7 for untreated wild-type, ASO-*Plp1*.a-treated *jimpy*, and ASO-*Plp1*.b-treated *jimpy* mice), and 6 month (n=5, 5, and 7 for untreated wild-type, ASO-*Plp1*.a-treated *jimpy*, and ASO-*Plp1*.b-treated *jimpy* mice) old mice by open field testing. Individual data points represent total distance traveled for each biological replicate (separate mice). Error bars show mean ± standard deviation. p-values calculated using one-way ANOVA with Dunnett's correction for multiple comparisons. See Supplementary Fig. 3 for raw data values.

862   **EXTENDED DATA FIGURE 1**

863
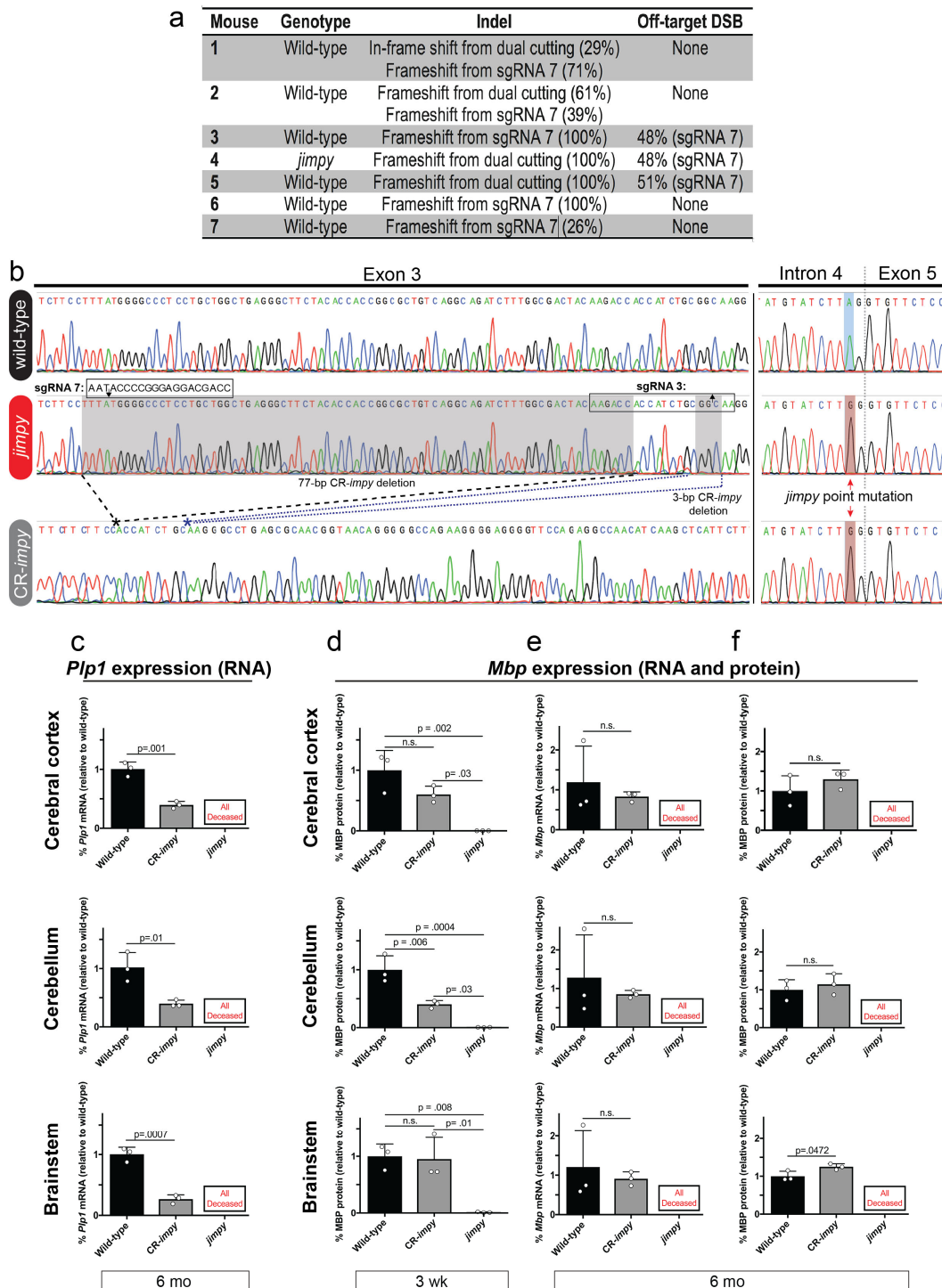
Extended Data Fig. 1 | CRISPR-mediated knockdown of *Plp1* in *jimpy* mice increases MBP transcript and protein levels.

a, Table showing the on- and off-target mutations for sgRNAs 3 and 7 after electroporation into mouse zygotes and measured by high-throughput sequencing of tail tip DNA from founder

870   animals. Mouse number 4, a *jimpy* male with a complex, frameshift deletion including 80-bp of
871   total deleted sequence in *Plp1* exon 3, served as the founder for the CR-*impy* cohort.

872   **b,** Annotated Sanger sequencing traces of wild-type, *jimpy,* and CR-*impy* mice showing the
873   complex, frameshift in *Plp1* exon 3 from dual cutting of CRISPR/spCas9 sgRNAs in CR-*impy*
874   mice as well as the *jimpy* point mutation in intron 4. sgRNA 3 and 7 sequences outlined by black
875   boxes with the predicted double strand break site shown a black arrow.

876   **c,** RT-qPCR data comparing the level of *Plp1* transcript in 6 month old CR-*impy* mice relative to
877   wild-type mice in three different brain regions (cerebral cortex, cerebellum, and brainstem). Primer
878   sites span *Plp1* exons 2-3, upstream of CR-*impy* complex, frameshift deletion and *jimpy* mutation
879   sites. Individual data points represent the mean value of 4 technical replicates for each biological
880   replicate (n=3 separate mice). Error bars show mean ± standard deviation. p-values calculated
881   using a two-way, unpaired t-test.

882   **d,** Western blot data comparing the level MBP in 3 week old CR-*impy* and *jimpy* mice relative to
883   wild-type mice across three different brain regions (cerebral cortex, cerebellum, and brainstem).
884   n=3 biological replicates (separate mice) per genotype (see Supplementary Fig. 2 for full western
885   blot images for all samples). Error bars show mean ± standard deviation. p-values calculated using
886   a one-way ANOVA with Tukey correction for multiple comparisons.

887   **e,** RT-qPCR data comparing the level of *Mbp* transcript in 6 month old CR-*impy* mice relative to
888   wild-type mice in three different brain regions (cerebral cortex, cerebellum, and brainstem).
889   Individual data points represent the mean value of 4 technical replicates for each biological
890   replicate (n=3 separate mice). Error bars show mean ± standard deviation. p-values calculated
891   using a two-way, unpaired t-test.

892   **f,** Western blot data comparing the level MBP in 6 month old CR-*impy* mice relative to wild-type
893   mice in three different brain regions (cerebral cortex, cerebellum, and brainstem). n=3 biological
894   replicates (separate mice) per genotype (see Supplementary Fig. 2 for full western blot images for
895   all samples). Error bars show mean ± standard deviation. p-values calculated using a two-way,
896   unpaired t-test.

897   **EXTENDED DATA FIGURE 2**

898

899
900
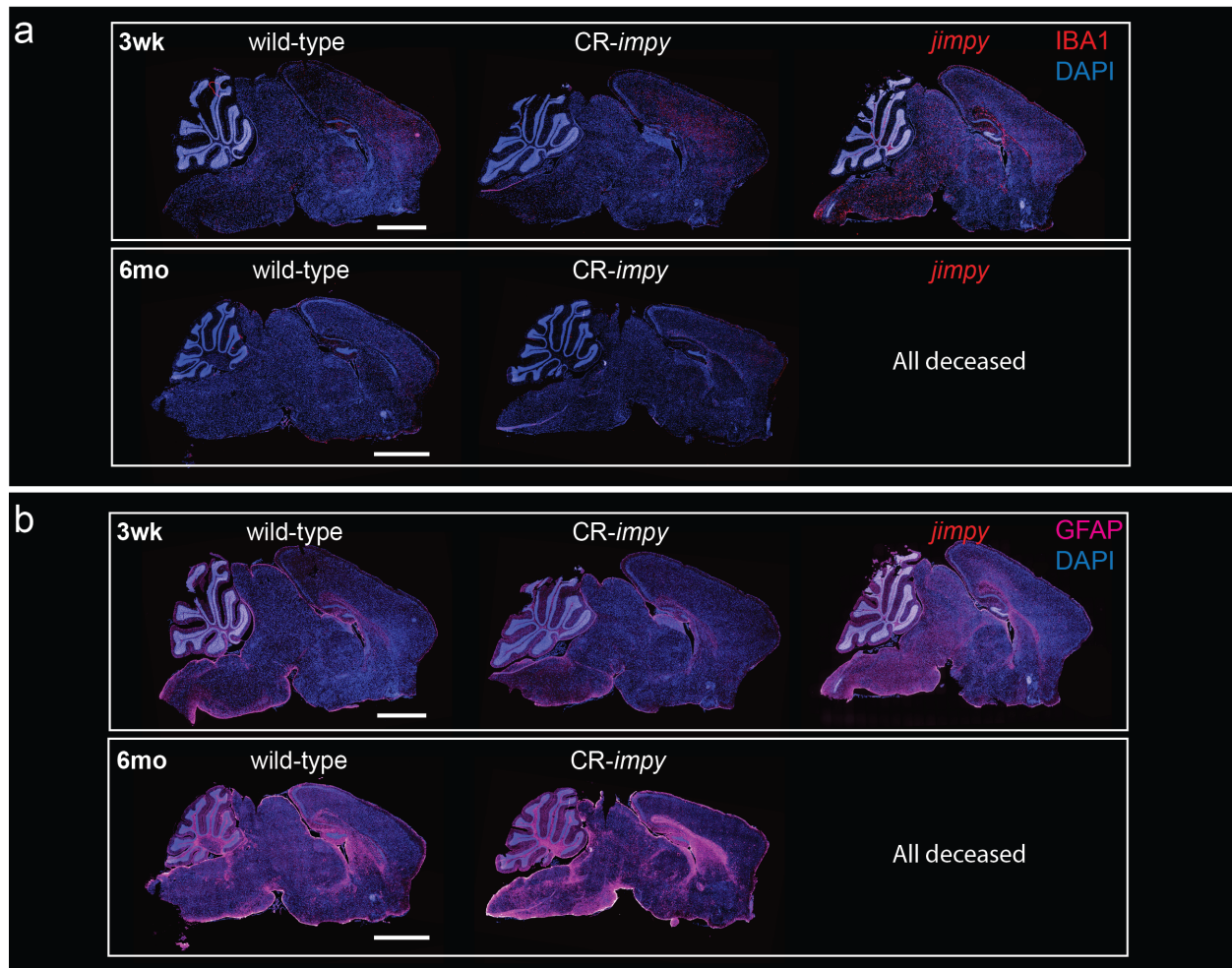
901   **Extended Data Fig. 2 | CRISPR-mediated knockdown of *Plp1* in *jimpy* mice reduces activated**
902   **microglia and astrocyte markers.**
903   **a,** Representative immunohistochemical images of whole-brain sagittal sections showing IBA1+
904   activated microglia (red), and total DAPI+ cells (blue) in wild-type, CR-*impy,* and *jimpy* mice at
905   3 weeks and 6 months of age as indicated. Scale bar, 2mm.
906   **b,** Representative immunohistochemical images of whole-brain sagittal sections showing GFAP+
907   astrocytes (magenta), and total DAPI+ cells (blue) in wild-type, CR-*impy*, and *jimpy* mice at 3
908   weeks and 6 months of age as indicated. Scale bar, 2mm.

38

909   **EXTENDED DATA FIGURE 3**

910

911
912
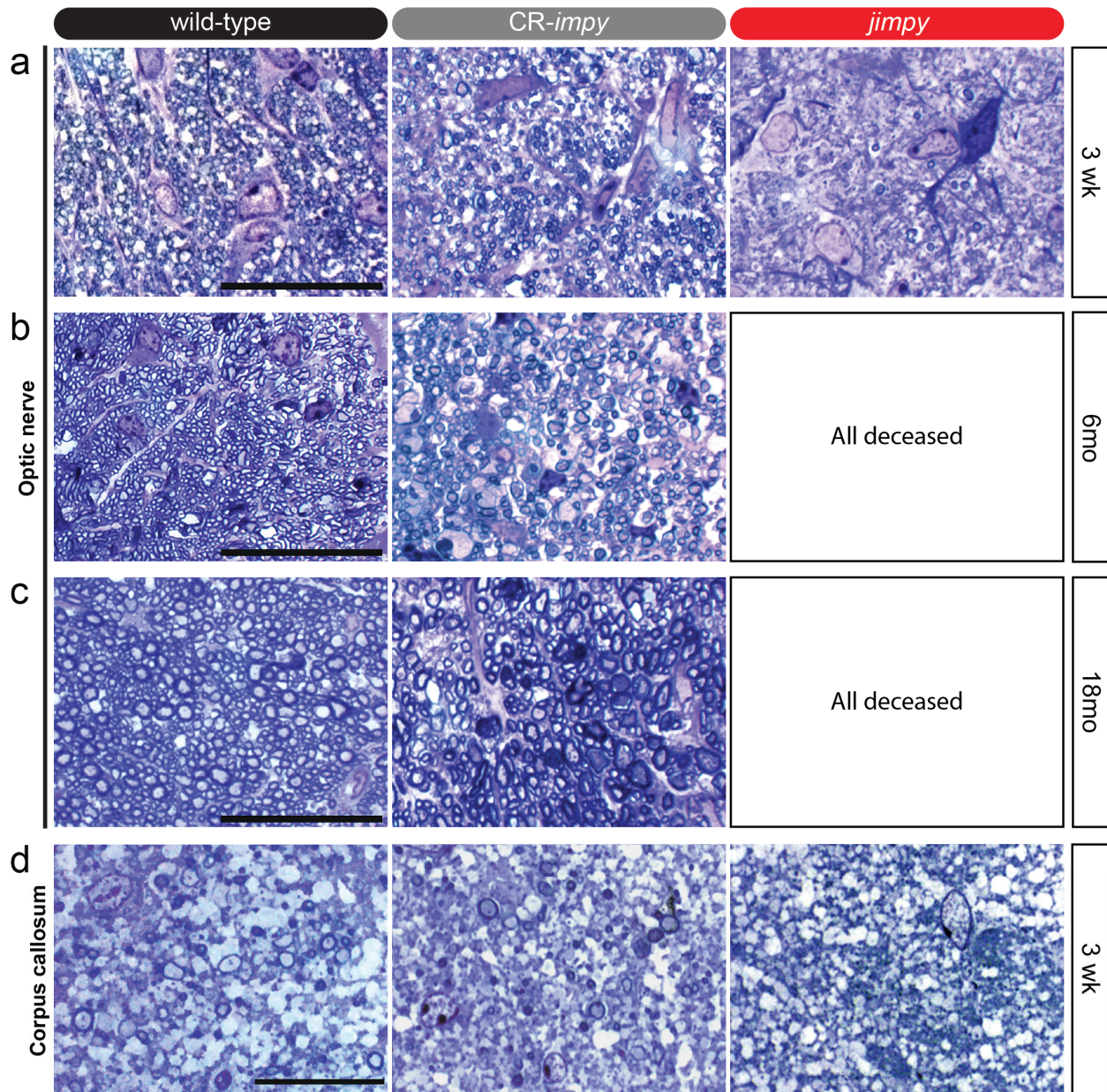
Extended Data Fig. 3 | CRISPR-mediated knockdown of *Plp1* in *jimpy* mice increases myelination.

a, Representative images of toluidine blue-stained optic nerve sections from 3 week old wild-type, CR-*impy*, and *jimpy* mice. Scale bar, 20μm.

b-c, Representative images of toluidine blue-stained optic nerve sections from 6 month (b) and 18 month (c) old wild-type, CR-*impy*, and *jimpy* mice. Scale bar, 20μm.

d, Representative images of toluidine blue-stained corpus callosum sections from 3 week old wild-type, CR-*impy*, and *jimpy* mice. Scale bar, 20μm.

EXTENDED DATA FIGURE 4
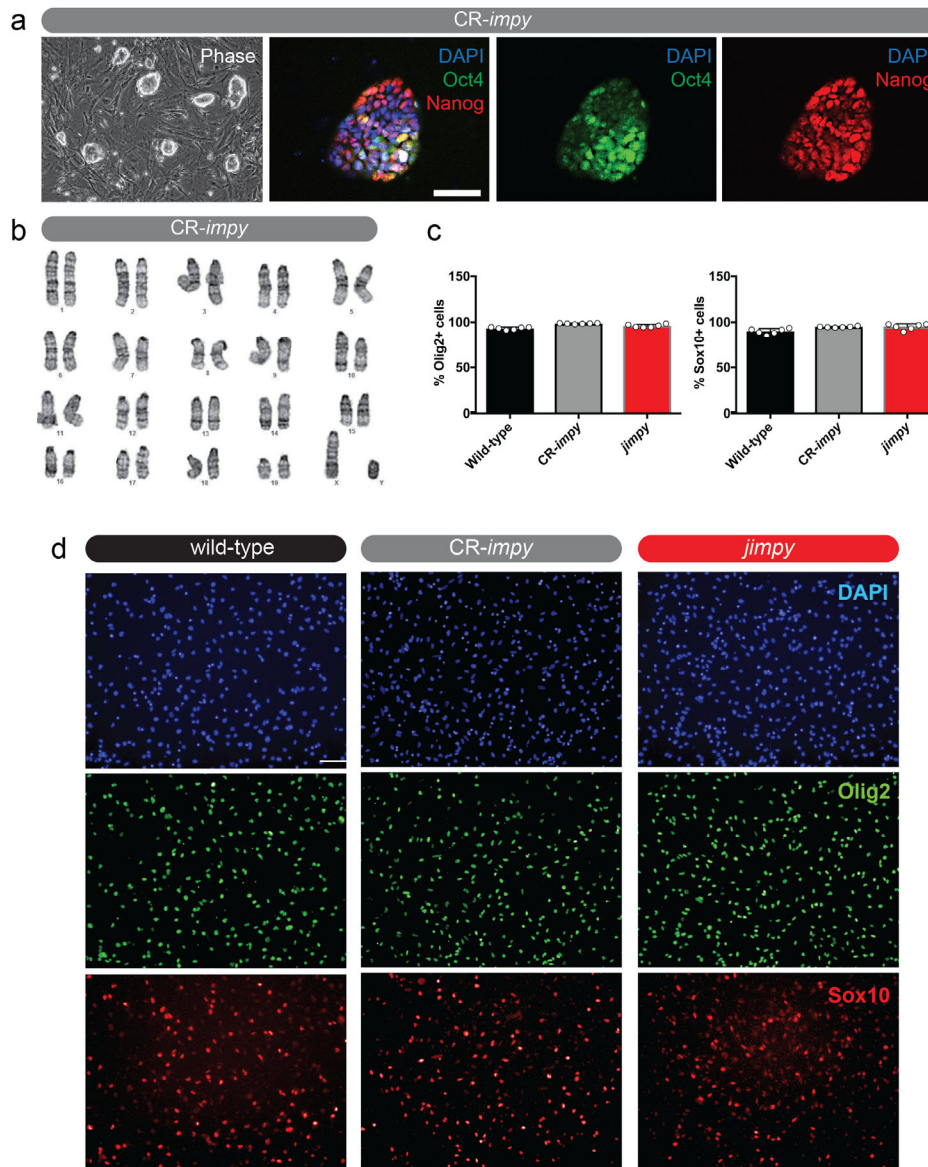
Extended Data Fig. 4 | Characterization of mouse iPSC lines and derivation of OPCs.

a, Representative phase and immunocytochemistry images of Oct4+ (green) and Nanog+ (red) iPSCs reprogrammed from CR-*impy*, tail-tip fibroblasts. Scale bar, 50um.

b, Normal karyotype of CR-*impy* iPSC line used to generate OPCs.

c, Percentage of Sox10+ and Olig2+ cells in OPCs cultures from wild-type, CR-*impy*, and *jimpy* iPSCs. Error bars show mean ± standard deviation. n=6 technical replicates (single cell line per genotype with 6 separate wells scored).

d, Representative immunocytochemistry images showing relative purity of Olig2+ and Sox10+ OPCs derived from wild-type, CR-*impy*, and *jimpy* iPSCs. Scale bar, 100um.

EXTENDED DATA FIGURE 5
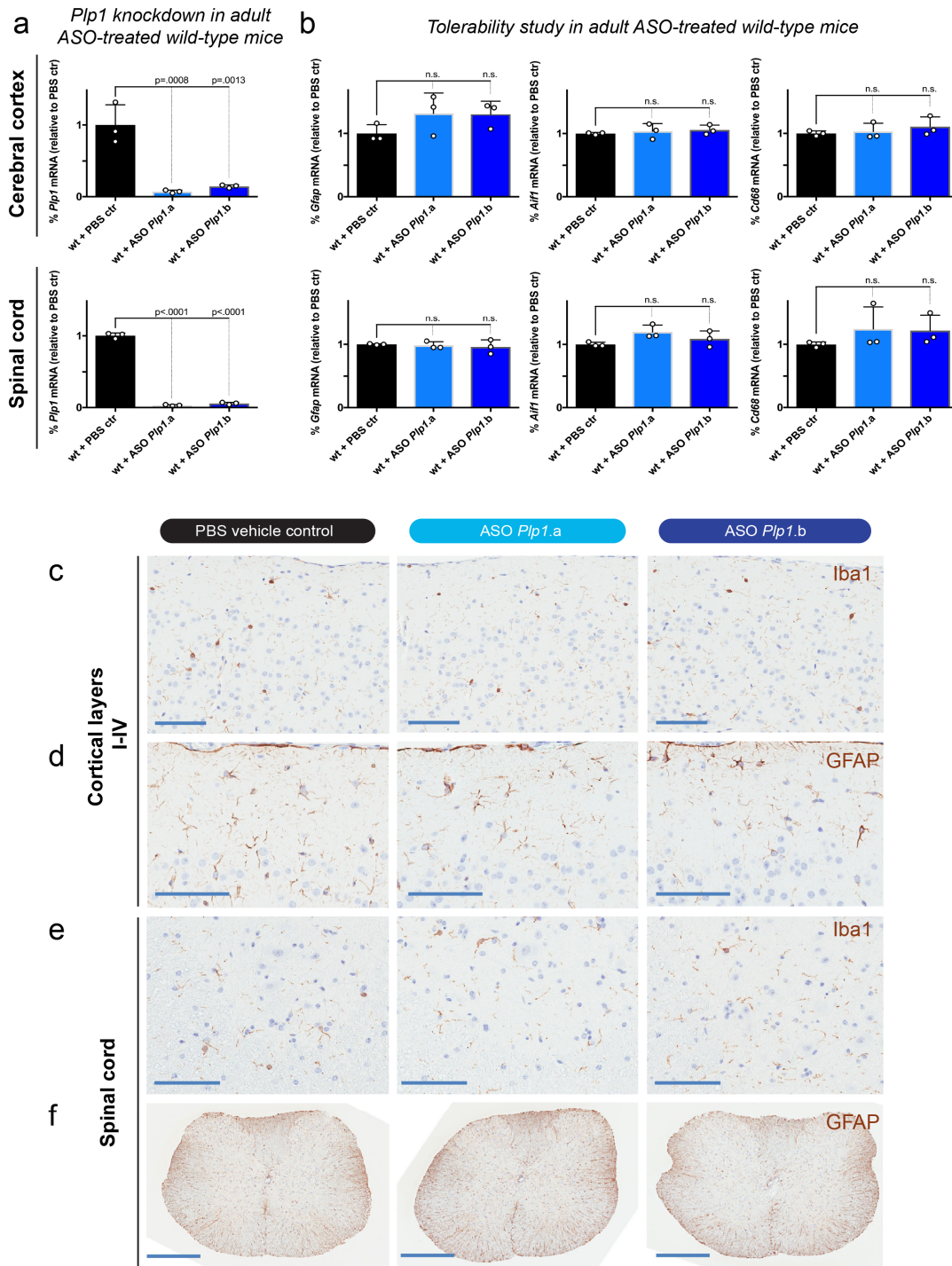
Extended Data Fig. 5 | *Plp1*-targeted ASOs show robust and sustained *Plp1* suppression and do not alter markers of glial activation/recruitment in wild-type adult mouse CNS.
a, RT-qPCR data comparing the level of *Plp1* transcript suppression in 16 week old cerebral cortex and spinal cord of wild-type mice treated with the indicated ASOs (300ug dose) or controls at

942   week 8. Individual data points represent the mean value of 3 technical replicates for each biological
943   replicate (n=3 separate mice). Error bars show mean ± standard deviation. p-values calculated
944   using one-way ANOVA with Dunnett's correction for multiple comparisons.
945   **b,** RT-qPCR data assessing ASO tolerability by expression levels of *Gfap* (astrocyte marker)*, Aif1*
946   (microglia marker)*, and Cd68* (monocyte/macrophage marker) transcripts in 16 week old cerebral
947   cortex and spinal cord of wild-type mice treated with the indicated ASOs (300ug dose) or controls
948   at week 8. Individual data points represent the mean value of 3 technical replicates for each
949   biological replicate (n=3 separate mice). Error bars show mean ± standard deviation. p-values
950   calculated using one-way ANOVA with Dunnett's correction for multiple comparisons.
951   **c-f,** Iba1 or GFAP immunohistochemistry (brown) with hematoxylin counterstain (purple)
952   showing no appreciable increase among groups in staining intensity, cellularity, or shortened, thick
953   processes that would be consistent with glial activation. (c) cortical layers I-IV Iba1 staining, scale
954   bar = 100 μm (d) cortical layers I-III GFAP staining, scale bar = 100 μm. (e) spinal cord dorsal
955   horn grey/white matter intersection Iba1 staining, scale bar = 100 μm. (f) Spinal cord GFAP
956   staining, scale bar = 500 μm.

957 **EXTENDED DATA FIGURE 6**

958
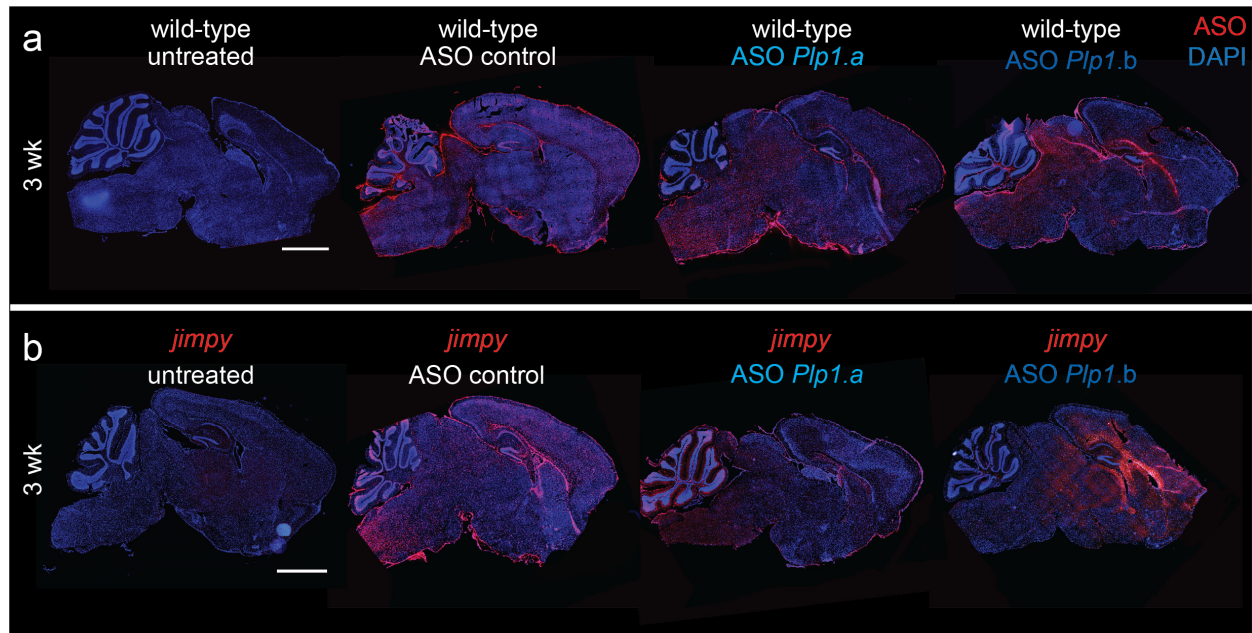
Extended Data Fig. 6 | *Plp1*-targeted ASOs distribute widely throughout the CNS after ICV dosing in postnatal mice.
a-b, Representative immunohistochemical images of 3 week whole-brain sagittal sections showing ASO (red) and total DAPI+ cells (blue) in wild-type mice (a) or *jimpy* (b) mice treated with ASO-*Plp1*.a, ASO-*Plp1*.b, or a control ASO by ICV injection at birth. Scale bar, 2mm.

EXTENDED DATA FIGURE 7

Plp1 expression (RNA & Protein)   **Mbp expression (RNA & Protein)**
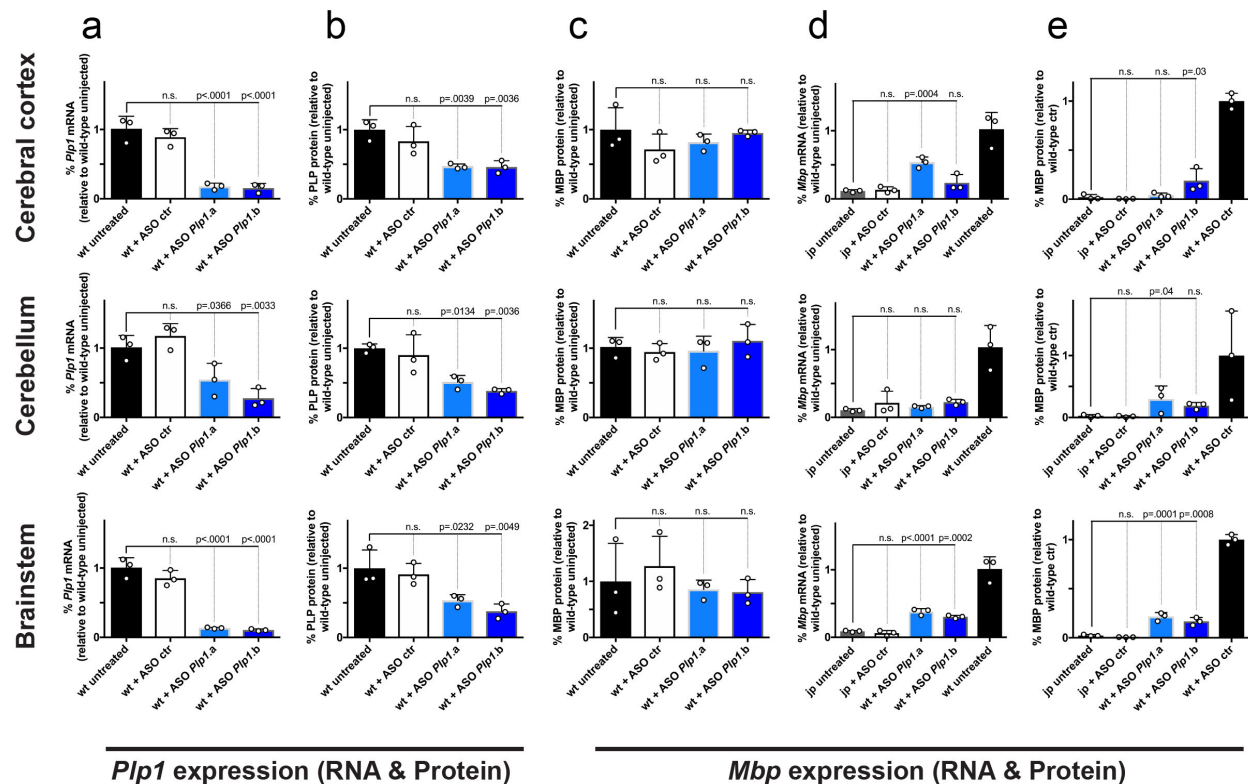
Extended Data Fig. 7 | Plp1-targeted ASOs increase MBP transcript and protein levels in jimpy mice.

a, RT-qPCR data showing the level of Plp1 transcript suppression in 3 week old cerebral cortex, cerebellum, and brainstem of wild-type mice treated with the indicated ASOs (30ug dose) or controls at birth. Primer sites span Plp1 exons 2-3, upstream of the jimpy mutation site. Individual data points represent the mean value of 4 technical replicates for each biological replicate (n=3 separate mice). Error bars show mean ± standard deviation. p-values calculated using one-way ANOVA with Dunnett's correction for multiple comparisons.

b, Western blot data showing the levels of PLP in 3 week old cerebral cortex, cerebellum, and brainstem of wild-type mice treated with the indicated ASOs (30ug dose) or controls at birth. Individual data points represent biological replicates (n=3 separate mice; see Supplementary Fig. 4 for full western blot images for all samples). Error bars show mean ± standard deviation. p-values calculated using one-way ANOVA with Dunnett's correction for multiple comparisons.

c, Western blot data showing the levels of MBP in 3 week old cerebral cortex, cerebellum, and brainstem of wild-type mice treated with the indicated ASOs (30ug dose) or controls at birth. Individual data points represent biological replicates (n=3 separate mice; see Supplementary Fig. 4 for full western blot images for all samples). Error bars show mean ± standard deviation. p-values calculated using one-way ANOVA with Dunnett's correction for multiple comparisons.

d, RT-qPCR data showing the level of Mbp transcript in 3 week old cerebral cortex, cerebellum, and brainstem of jimpy mice treated with the indicated ASOs (30ug dose) or controls at birth.

44

990   Individual data points represent the mean value of 4 technical replicates for each biological
991   replicate (n=3 separate mice). Error bars show mean ± standard deviation. p-values calculated
992   using one-way ANOVA with Dunnett's correction for multiple comparisons.
993   **e,** Western blot data showing the level of MBP in 3 week old cerebral cortex, cerebellum, and
994   brainstem of *jimpy* mice treated with the indicated ASOs (30ug dose) or controls at birth.
995   Individual data points represent biological replicates (n=3 separate mice; see Supplementary Fig.
996   4 for full western blot images for all samples). Error bars show mean ± standard deviation. p-
997   values calculated using one-way ANOVA with Dunnett's correction for multiple comparisons.

998 **EXTENDED DATA TABLE 1**

999

PLP1 mutation	Patient #	Motor function	Cognitive function	Death	Ref.
Frameshift and early termination codon (c.4delG) *Protein absence confirmed by western blot*	1	Wheelchair bound at 35 with spasticity in all limbs	No intellectual disability and verbally communicated into mid-20s. Cooperative, alert, and aware of surroundings in adulthood.	Age 47	(*1, 2*)
	2	Wheelchair bound at 37 with spasticity in all limbs	No intellectual disability and verbally communicated into mid-20s. Cooperative, alert, and aware of surroundings in adulthood.	Age 49	
	3	Walked from age 4-12, spasticity in all limbs at age 25	Language delay. At 22 communicated, was cooperative, and alert. At 25 could follow commands, count, and distinguish colors.	Age 34	
	4	Wheelchair bound at 17, gait deterioration starting at age 8, and spasticity in legs but not arms.	Able to read, follow commands, and perform arithmetic.	None reported	
Frameshift and early termination codon c.191+1G>A *No biochemical analysis*	1	Walked from age 6-9. Spastic with cerebellar dysfunction.	Attends normal school and can read and write.	None reported	(*3*)
Loss of start codon (c.3G>A) *No biochemical analysis*	1	Early life motor dysfunction with spasticity in arms and legs. Further decline at age 33.	Early life intellectual disability. Further decline at age 33.	None reported	(*2, 4*)
	2	Early life hypertonia and spasticity in arms and legs. Wheelchair bound at 6.	Language delay. Moderately retarded development.	None reported	
	3	Never walked and spasticity in legs by age 1, progressing to arms with age.	Mild cognitive deficits at age 20.	None reported	(*5*)

1000

1001 **Extended Data Table 1**

1002 Table containing details of published reports of *PLP1*-null patients.

SUPPLEMENTARY FIGURE 1

Metadata for mouse CRISPR survival cohort from Elitt et al. ver.12-25-18

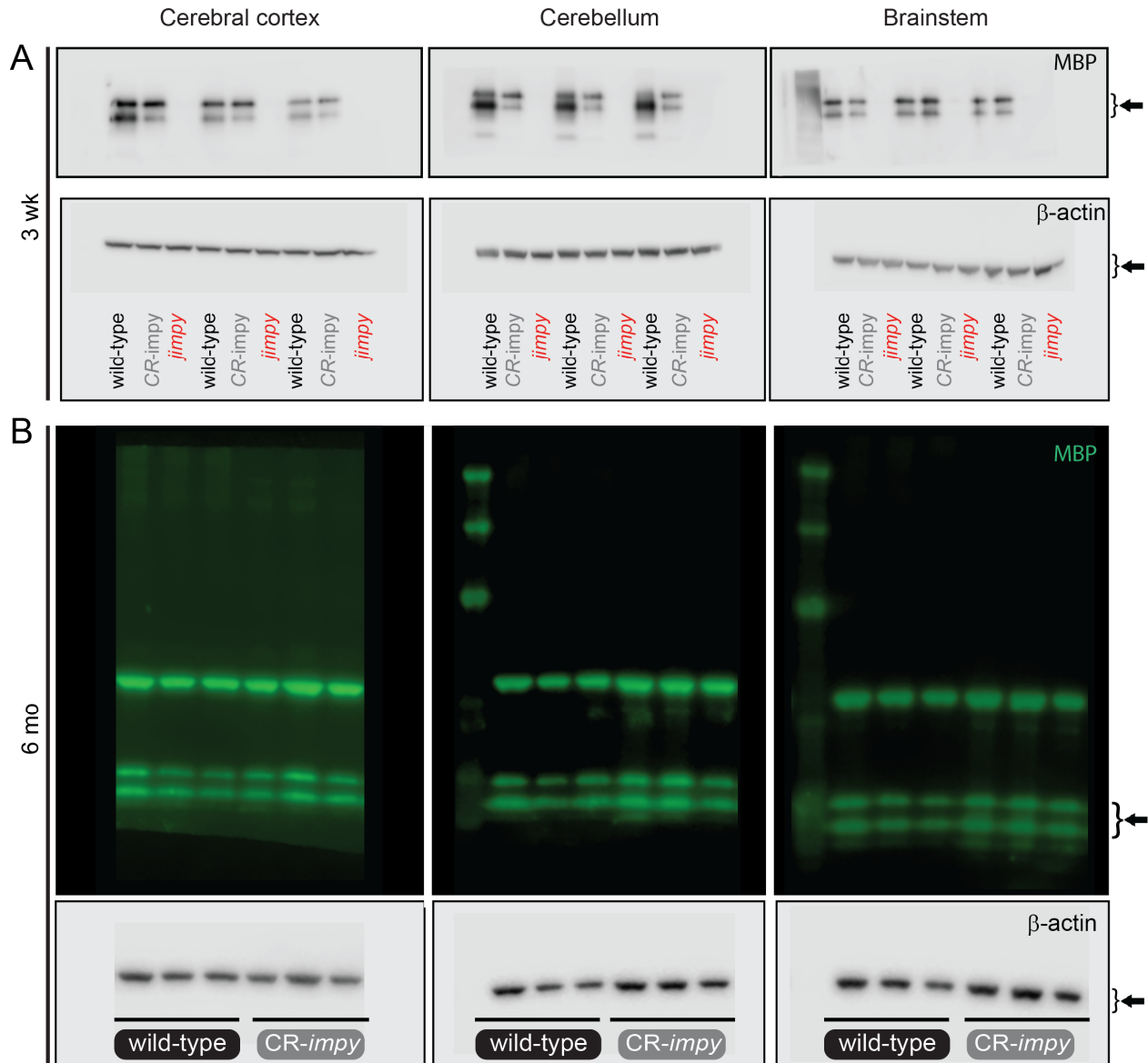mean time to fall (seconds)   total distance traveled (meters)

Identifier	Date of birth	Date of death	Euthanized at 18 month endpoint?	Lifespan (days)	Genotype	Phenotype	Censored (Y/N)	Censor Reason	Rotarod 3 wk	Rotarod 2 mo	Rotarod 6 mo	Rotarod 18 mo	Open field 3 wk	Open field 2 mo	Open field 6 mo	Open field 18 mo
CR200301	11/13/2016	4/22/2018	n	525	wild-type	none	N		69.3	70.9	61.8		22.8	17.9	12.5	
CR200090	11/13/2016	5/14/2018	y	547	wild-type	none	N		144.0	104.1	60.1	43.0	17.0	17.4	10.8	13.2
CR200091	11/13/2016	5/14/2018	y	547	wild-type	none	N		81.3	103.4	77.5	61.3	19.3	18.8	10.2	15.4
CR200302	11/15/2016	12/5/2017	n	385	CR-*impy*	none	N		100.7	120.9	108.0		10.9	15.0	15.5	
CR200303	11/15/2016	12/28/2017	n	408	CR-*impy*	none	N		115.3	138.0	74.2		8.6	14.3	17.7	
CR200304	11/15/2016	5/6/2018	n	537	CR-*impy*	none	N		95.7	138.3	55.2		13.7	11.0	11.5	
CR200092	11/15/2016	5/14/2018	y	545	CR-*impy*	none	N		139.4	106.3	66.2	16.3	10.1	10.2	10.5	7.3
CR200093	11/15/2016	5/14/2018	y	545	CR-*impy*	none	N		72.7	117.7	116.3	29.2	17.1	7.9	17.3	22.0
CR200305	11/15/2016	12/8/2016	n	23	*jimpy*	severe	N		39.1				3.9			
CR200306	11/15/2016	12/7/2016	n	22	*jimpy*	severe	N		21.0				2.4			
CR200307	11/15/2016	12/9/2016	n	24	*jimpy*	severe	N		20.7				1.0			
CR200308	11/15/2016	12/5/2016	n	20	*jimpy*	severe	N		12.9				5.5			
CR200309	11/15/2016	12/6/2016	n	21	*jimpy*	severe	N		4.7				6.8			
CR200310	11/16/2016	12/17/2016	n	31	*jimpy*	severe	N		38.7				0.4			
CR200311	11/16/2016	12/10/2016	n	24	*jimpy*	severe	N		31.9				0.6			
CR200312	11/17/2016	4/30/2018	n	529	wild-type	none	N		101.6	84.7	52.9		19.0	7.0	8.1	
CR200096	11/17/2016	5/14/2018	y	543	wild-type	none	N		93.0	219.3	125.7	29.1	20.0	25.7	12.7	12.5
CR200313	11/17/2016	3/27/2018	n	495	wild-type	none	N		156.7	70.4	52.6		14.4	17.0	9.3	
CR200097	11/17/2016	5/14/2018	y	543	wild-type	none	N		55.9	86.0	118.8	71.9	15.6	18.0	25.1	14.1
CR200094	11/18/2016	5/14/2018	y	542	CR-*impy*	none	N		65.8	74.0	111.1	16.3	22.5	15.8	16.2	7.2
CR200314	11/18/2016	3/19/2018	n	486	CR-*impy*	none	N		69.6	71.3	90.9		21.1	17.0	15.5	
CR200095	11/18/2016	5/14/2018	y	542	CR-*impy*	none	N		110.1	128.3	148.1	29.2	19.1	26.4	19.6	27.6
CR200315	11/26/2016	12/22/2016	n	26	*jimpy*	severe	N		2.7				1.8			
CR200316	11/26/2016	12/18/2016	n	22	*jimpy*	severe	N		27.3				0.5			
CR200317	11/26/2016	12/18/2016	n	22	*jimpy*	severe	N		24.2				0.9			
CR200318	11/26/2016	12/20/2016	n	24	*jimpy*	severe	N		26.9				1.2			
CR200319	11/26/2016	12/19/2016	n	23	*jimpy*	severe	N		41.4				1.0			
CR200320	12/12/2016	1/5/2017	n	24	*jimpy*	severe	N									
CR200321	12/12/2016	12/31/2016	n	19	*jimpy*	severe	N									
CR200322	12/12/2016	11/16/2017	n	339	CR-*impy*	none	N			102.9	88.2			25.229	26.0	
CR200323	12/12/2016	6/27/2018	y	562	CR-*impy*	none	N			81.1	89.4	43.9		15.418	17.8	19.6
CR200324	3/30/2017	4/20/2017	n	21	*jimpy*	severe	N									
CR200325	3/30/2017	4/20/2017	n	21	*jimpy*	severe	N									
CR200326	3/30/2017	4/26/2017	n	27	*jimpy*	severe	N									
CR200327	3/30/2017	4/24/2017	n	25	*jimpy*	severe	N									
CR200328	11/13/2016	10/1/2017	n	322	wild-type	none	Y	Euthanized inadvertantly	92.7	135.4	63.5		31.8	18.3	8.9	
CR200329	11/13/2016	10/1/2017	n	322	wild-type	none	Y	Euthanized inadvertantly	148.7	126.7	102.4		18.6	13.8	6.7	
CR200330	11/13/2016	10/1/2017	n	322	wild-type	none	Y	Euthanized inadvertantly	85.7	109.3	120.0		15.3	19.4	19.1	
CR200081	11/15/2016	6/1/2017	n	198	wild-type	none	Y	Tissue collection	196.0	160.7	145.0		13.5	20.9	10.3	
CR200082	11/15/2016	6/1/2017	n	198	CR-*impy*	none	Y	Tissue collection	132.3	91.5	99.1		13.5	15.1	20.3	
CR200083	11/15/2016	6/2/2017	n	199	CR-*impy*	none	Y	Tissue collection	120.5	93.6	96.9		21.5	23.7	25.2	
CR200084	11/15/2016	6/2/2017	n	199	wild-type	none	Y	Tissue collection	170.4	137.7	78.6		23.7	11.5	7.3	
CR200061	11/15/2016	5/25/2017	n	191	CR-*impy*	none	Y	Tissue collection	102.5	111.7	105.4		21.1	12.2	16.2	
CR200062	11/15/2016	5/25/2017	n	191	CR-*impy*	none	Y	Tissue collection	56.4	122.4	63.4		13.3	15.1	18.3	
CR200063	11/15/2016	5/25/2017	n	191	wild-type	none	Y	Tissue collection	109.3	115.3	57.3		26.3	26.3	10.8	
CR200064	11/15/2016	5/25/2017	n	191	wild-type	none	Y	Tissue collection	88.7	101.3	82.0		17.4	15.6	8.0	
CR200065	11/16/2016	5/30/2017	n	195	CR-*impy*	none	Y	Tissue collection	42.5	100.8	131.3		10.0	6.4	6.7	
CR200075	11/17/2016	5/31/2017	n	195	wild-type	none	Y	Tissue collection	82.1	32.1	23.3		24.0	21.3	21.1	
CR200076	11/17/2016	5/31/2017	n	195	wild-type	none	Y	Tissue collection	162.8	70.8	98.9		20.5	11.6	9.4	
CR200077	11/17/2016	5/31/2017	n	195	wild-type	none	Y	Tissue collection	120.6	95.5	108.5		20.5	26.0	14.1	
CR200078	11/18/2016	6/13/2017	n	207	CR-*impy*	none	Y	Tissue collection	40.5	102.0	97.6		19.7	13.0	7.8	
CR200079	11/18/2016	6/13/2017	n	207	wild-type	none	Y	Tissue collection	82.2	130.0	77.2		12.8	15.6	3.8	
CR200080	11/18/2016	6/12/2017	n	206	CR-*impy*	none	Y	Tissue collection	87.0	78.1	63.5		26.3	18.6	15.8	
CR200085	11/18/2016	6/12/2017	n	206	wild-type	none	Y	Tissue collection	75.8	113.4	104.0		19.7	9.3	8.3	
CR200071	11/18/2016	6/12/2017	n	206	CR-*impy*	none	Y	Tissue collection	59.0	142.3	134.3		8.0	16.5	8.3	
CR200086	11/18/2016	6/13/2017	n	207	CR-*impy*	none	Y	Tissue collection	79.7	112.2	100.1		14.3	8.512	12.0	
CR200098	11/18/2016	6/13/2017	n	207	wild-type	none	Y	Tissue collection	90.6	130.3	115.3		17.9	19.54	13.0	
CR200066	11/19/2016	5/30/2017	n	192	CR-*impy*	none	Y	Tissue collection	88.4	124.4	82.9		14.0	14.136	0.6	
CR200067	11/19/2016	5/30/2017	n	192	CR-*impy*	none	Y	Tissue collection	131.7	146.0	68.2		11.6	13.449	9.8	
CR200068	11/19/2016	5/30/2017	n	192	wild-type	none	Y	Tissue collection	82.5	119.3	126.1		14.1	20.689	14.5	
CR200069	11/22/2016	5/30/2017	n	189	wild-type	none	Y	Tissue collection	88.4	67.0	41.5		19.0	9.404	8.4	
CR200070	11/22/2016	5/30/2017	n	189	wild-type	none	Y	Tissue collection	88.3	80.6	77.4		20.1	9.051	5.2	
CR200072	11/22/2016	6/1/2017	n	191	wild-type	none	Y	Tissue collection	110.7	170.0	124.3		21.7	19.759	11.8	
CR200073	11/22/2016	6/1/2017	n	191	wild-type	none	Y	Tissue collection	145.0	152.3	116.1		13.5	22.028	11.4	
CR200331	11/26/2016	5/23/2017	n	178	CR-*impy*	none	Y	Euthanized inadvertantly	110.0	196.0			24.3	16.452		
CR200074	12/12/2016	6/1/2017	n	171	CR-*impy*	none	Y	Tissue collection		94.2				23.557		

Supplementary Figure 1

Table of metadata for all mice in Kaplan-Meier survival plot in Fig. 1b. Also included are raw data values for rotarod and open field assays in Fig. 2c, d.

SUPPLEMENTARY FIGURE 2

Supplementary Figure 2
a-b, Labeled raw images of western blots for all samples in Extended Data Figs. 1d, f. The upper bands in the fluorescent blots in panel B are carry over from chemiluminescent detection of B-actin (bottom panel).
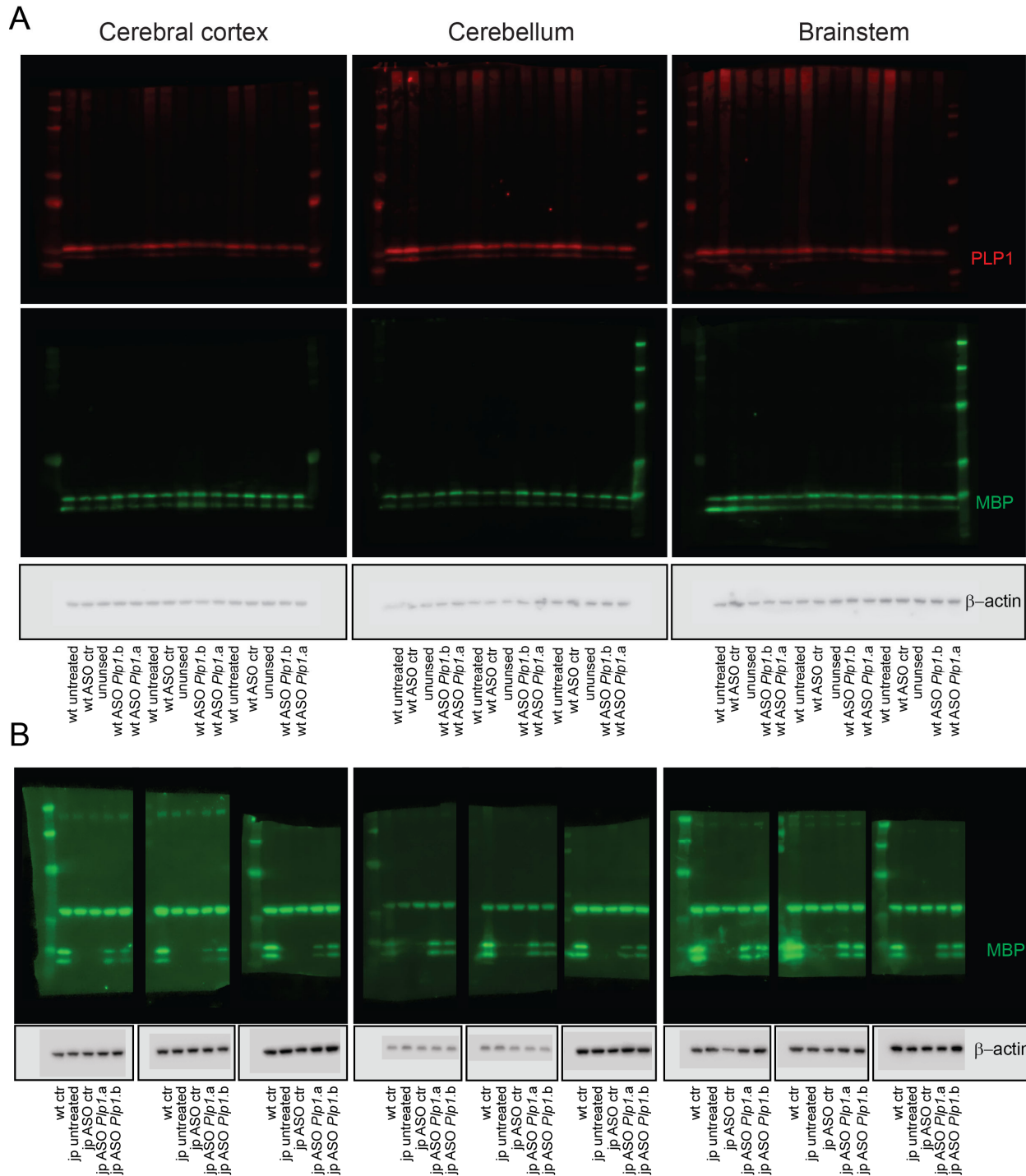
SUPPLEMENTARY FIGURE 3

Metadata for mouse ASO survival cohort from Elitt et al. ver.12-25-18

Identifier	Date of birth	Date of death	Euthanized at 8 month endpoint?	Lifespan (days)	Genotype	Treatment	Phenotype	Additional phenotype notes	mean time to fall (seconds) Rotarod 2 mo	Rotarod 4 mo	Rotarod 6 mo	total distance traveled (meters) Open field 2 mo	Open field 4 mo	Open field 6 mo
ASO00091	11/23/2017	7/20/2018	y	239	jimpy	ASO Plp1.a	mild	Periorbital area inflammation, left eye	32.9	22.4	5.6	22.0	18.0	18.0
ASO00095	11/23/2017	7/20/2018	y	239	jimpy	ASO Plp1.a	mild	Periorbital area inflammation, bilateral	22.3	24.6	unable to train	19.6	13.7	14.0
ASO000S1	12/7/2017	12/28/2017	n	21	jimpy	uninjected	severe							
ASO000S2	12/7/2017	12/28/2017	n	21	jimpy	ASO control	severe							
ASO000S3	12/7/2017	12/29/2017	n	22	jimpy	ASO control	severe							
ASO000S4	12/7/2017	12/27/2017	n	20	jimpy	ASO control	severe							
ASO000S5	12/8/2017	12/24/2017	n	16	jimpy	uninjected	severe							
ASO000S6	12/8/2017	12/27/2017	n	19	jimpy	uninjected	severe							
ASO000S7	12/11/2017	12/26/2017	n	15	jimpy	uninjected	severe							
ASO000S8	12/5/2017	12/25/2017	n	20	jimpy	uninjected	severe							
ASO000S9	12/5/2017	12/25/2017	n	20	jimpy	uninjected	severe							
ASO000S10	12/8/2017	12/28/2017	n	20	jimpy	uninjected	severe	Found with hind-limb paralysis, required euthanization						
ASO000S11	12/8/2017	12/30/2017	n	22	jimpy	uninjected	severe							
ASO000S12	12/8/2017	12/28/2017	n	20	jimpy	uninjected	severe	Found with hind-limb paralysis, required euthanization						
AS000103	12/27/2017	8/27/2018	y	243	jimpy	ASO Plp1.b	mild	Periorbital area inflammation, right eye	unable to train	unable to train	unable to train	13.2	6.2	4.3
AS000104	12/27/2017	8/27/2018	y	243	jimpy	ASO Plp1.b	mild		39.4	49.5	27.8	14.5	9.0	11.3
ASO000S13	12/27/2017	1/18/2018	n	22	jimpy	uninjected	severe							
AS000105b	12/28/2017	8/27/2018	y	242	jimpy	ASO Plp1.b	mild		51.5	37.2	36.9	13.8	12.7	8.8
AS000106	12/28/2017	8/27/2018	y	242	jimpy	ASO Plp1.b	mild		34.7	27.4	37.2	15.0	15.5	8.9
AS000107	12/30/2017	8/27/2018	y	240	jimpy	ASO Plp1.a	mild		unable to train	unable to train	unable to train	11.3	15.7	12.8
AS000108	12/30/2017	8/27/2018	y	240	jimpy	ASO Plp1.a	mild	Periorbital area inflammation, bilateral	unable to train	17.0	unable to train	10.1	15.1	18.5
AS000109	12/31/2017	8/27/2018	y	239	jimpy	ASO Plp1.a	mild		14.3	34.1	3.3	15.1	14.2	10.7
ASO000S14	12/18/2017	1/5/2018	n	18	jimpy	uninjected	severe							
ASO000S15	12/18/2017	1/5/2018	n	18	jimpy	uninjected	severe							
ASO000S16	12/18/2017	1/4/2018	n	17	jimpy	uninjected	severe							
ASO000S17	1/6/2018	1/25/2018	n	19	jimpy	ASO control	severe							
ASO000S18	1/6/2018	1/25/2018	n	19	jimpy	ASO control	severe							
ASO000S19	12/29/2017	1/18/2018	n	20	jimpy	uninjected	severe							
AS000115	1/22/2018	9/7/2018	y	228	jimpy	ASO Plp1.b	mild		41.9	19.2	8.1	11.9	8.4	3.3
ASO000S20	1/22/2018	3/30/2018	n	67	jimpy	ASO Plp1.b	mild		31.1	dead	dead	20.5	dead	dead
AS000117	1/22/2018	9/7/2018	y	228	jimpy	ASO Plp1.b	mild		40.1	unable to train	unable to train	14.8	16.4	18.6
AS000110	1/18/2018	9/17/2018	y	242	jimpy	ASO Plp1.b	mild	Upper back inflammation	unable to train	unable to train	unable to train	23.9	25.2	17.3
ASO000096	12/7/2017	7/23/2018	y	228	wild-type	ASO control	none							
ASO000097	12/7/2017	7/23/2018	y	228	wild-type	ASO control	none							
ASO000099	12/7/2017	7/23/2018	y	228	wild-type	ASO control	none							
AS000100	12/5/2017	7/23/2018	y	230	wild-type	uninjected	none		111.1	110.8	63.7	8.2	1.4	3.9
AS000101	12/5/2017	7/23/2018	y	230	wild-type	uninjected	none		76.8	94.9	64.6	12.0	3.3	2.9
AS000102	12/5/2017	7/23/2018	y	230	wild-type	uninjected	none		53.1	54.3	67.0	8.0	7.9	3.8
AS000111	1/19/2018	9/17/2018	y	241	wild-type	uninjected	none		84.0	80.5	67.4	37.2	32.9	21.7
AS000112	1/19/2018	9/17/2018	y	241	wild-type	uninjected	none		107.0	61.0	76.3	17.9	7.5	6.2
AS000122	4/5/2018	12/14/2018	y	253	wild-type	ASO control	none				3.7			14.3
AS000123	4/5/2018	12/14/2018	y	253	wild-type	ASO control	none				18.3			1.8
AS000124	4/5/2018	12/14/2018	y	253	wild-type	ASO control	none				89.4			20.5
AS000125	4/5/2018	12/14/2018	y	253	wild-type	ASO control	none				107.1			13.2
AS000126	4/13/2018	12/13/2018	y	244	wild-type	ASO control	none				123.7			13.0
AS000127	4/13/2018	12/13/2018	y	244	wild-type	ASO control	none				45.4			20.4
AS000128	4/14/2018	12/14/2018	y	244	wild-type	ASO control	none							
ASO000S21	5/4/2018	ongoing (still alive)			wild-type	ASO control	none							
ASO000S22	5/4/2018				wild-type	ASO control	none							

Supplementary Figure 3

Table of metadata for all mice in Kaplan-Meier survival plot in Fig. 4c (as of 12-25-18 with two mice not yet at the 8 month endpoint). We noted 5 of 13 of ASO-treated *jimpy* mice in our survival cohort developed periorbital or upper back skin inflammation. The underlying cause of this is unknown as it was not observed in ASO treated wild-type littermates. Also included are raw data values for rotarod and open field assays in Fig. 4i, j.

SUPPLEMENTARY FIGURE 4

Supplementary Figure 4

a-b, Labeled raw images of western blots for all samples in Extended Data Figs. 7b, c, e. The upper bands in the fluorescent blots in panel B are carry over from chemiluminescent detection of B-actin (bottom panel).

1036 **SUPPLEMENTARY VIDEOS 1-4 (four separate MP4 files)**

1037

1038 **Supplementary Video 1 | CRISPR-mediated knockdown of *Plp1* in *jimpy* mice rescues**
1039 **neurological phenotypes at 3 weeks of age.**
1040 Video comparison of wild-type, *jimpy*, and CR-*impy* mice at 3 weeks of age.

1041

1042 **Supplementary Video 2 | CRISPR-mediated knockdown of *Plp1* in *jimpy* mice shows**
1043 **sustained rescue of neurological phenotypes at 18 months of age.**
1044 Video comparison of wild-type and CR-*impy* mice at 18 weeks of age (study endpoint).

1045

1046 **Supplementary Video 3 | Postnatal delivery of *Plp1*-targeted ASOs to *jimpy* mice rescues**
1047 **neurological phenotypes at 3 weeks of age.**
1048 Video comparison of wild-type and *jimpy* mice treated with control and *Plp1*-targeting ASOs at 3
1049 weeks of age.

1050

1051 **Supplementary Video 4 | Postnatal delivery of *Plp1*-targeted ASOs to *jimpy* mice shows**
1052 **sustained rescue of neurological phenotypes at 6 months of age.**
1053 Video comparison of wild-type and *jimpy* mice treated with control and *Plp1*-targeting ASOs at 6
1054 months of age.

Supplementary References

1055   1.   J. Y. Garbern *et al.*, Proteolipid protein is necessary in peripheral as well as central myelin. *Neuron* **19**, 205-218 (1997).

2.   J. Y. Garbern *et al.*, Patients lacking the major CNS myelin protein, proteolipid protein 1, develop length-dependent axonal degeneration in the absence of demyelination and inflammation. *Brain* **125**, 551-561 (2002).

3.   P. Lassuthova *et al.*, Three new PLP1 splicing mutations demonstrate pathogenic and phenotypic diversity of Pelizaeus-Merzbacher disease. *Journal of child neurology* **29**, 924-931 (2014).

4.   E. A. Sistermans *et al.*, A (G-to-A) mutation in the initiation codon of the proteolipid protein gene causing a relatively mild form of Pelizaeus-Merzbacher disease in a Dutch family. *Hum Genet* **97**, 337-339 (1996).

5.   C. K. Hand, G. Bernard, M.-P. Dubé, M. I. Shevell, G. A. Rouleau, A Novel PLP1 Mutation Further Expands the Clinical Heterogeneity at the Locus. *The Canadian Journal of Neurological Sciences* **39**, 220-224 (2014).